105. Lovell, W. G.: "Knocking Characteristics of Hydrocarbons," *Ind. Engng. Chem.*, vol. 40, pp. 2388–2438, 1948.
106. Lichty, L. C.: *Combustion Engine Processes*, McGraw-Hill, 1967.
107. Ethyl Corporation: "Determining Road Octane Numbers," Ethyl technical note PCDTN SP-347 (113) Rev. 573.
108. Benson, J.: "What Good are Octanes," in *Chemtech*, pp. 16–22, American Chemical Society, January 1976.
109. Barusch, M. R., Macpherson, J. B., and Amberg, G. H.: "Additives, Engine Fuel," in J. J. McKetta and W. A. Cunningham (eds.), *Encyclopedia of Chemical Processing and Design*, vol. 2, pp. 1–77, Marcel Dekker, New York and Basel, 1977.
110. McCabe, L. J., Fitch, F. B., and Lowther, H. V.: "Future Trends in Automotive Fuels and Engine Oils," SAE paper 830935, in *Proceedings of Second International Pacific Conference on Automotive Engineering*, pp. 678–697, Tokyo, Japan, Nov. 7–10, 1983.
111. Benson, J. D.: "Some Factors Which Affect Octane Requirement Increase," SAE paper 750933, *SAE Trans.*, vol. 84, 1975.

# CHAPTER 10

# COMBUSTION IN COMPRESSION-IGNITION ENGINES

## 10.1 ESSENTIAL FEATURES OF PROCESS

The essential features of the compression-ignition or diesel engine combustion process can be summarized as follows. Fuel is injected by the fuel-injection system into the engine cylinder toward the end of the compression stroke, just before the desired start of combustion. Figures 1-17, 1-18, and 1-19 illustrate the major components of common diesel fuel-injection systems. The liquid fuel, usually injected at high velocity as one or more jets through small orifices or nozzles in the injector tip, atomizes into small drops and penetrates into the combustion chamber. The fuel vaporizes and mixes with the high-temperature high-pressure cylinder air. Since the air temperature and pressure are above the fuel's ignition point, spontaneous ignition of portions of the already-mixed fuel and air occurs after a delay period of a few crank angle degrees. The cylinder pressure increases as combustion of the fuel-air mixture occurs. The consequent compression of the unburned portion of the charge shortens the delay before ignition for the fuel and air which has mixed to within combustible limits, which then burns rapidly. It also reduces the evaporation time of the remaining liquid fuel. Injection continues until the desired amount of fuel has entered the cylinder. Atomization, vaporization, fuel-air mixing, and combustion continue until essentially all the fuel has passed through each process. In addition, mixing of the air remaining in the cylinder with burning and already burned gases continues throughout the combustion and expansion processes.

It will be clear from this summary that the compression-ignition combustion process is extremely complex. The details of the process depend on the characteristics of the fuel, on the design of the engine's combustion chamber and fuel-injection system, and on the engine's operating conditions. It is an unsteady, heterogeneous, three-dimensional combustion process. While an adequate conceptual understanding of diesel engine combustion has been developed, to date an ability to describe many of the critical individual processes in a quantitative manner is lacking.

Some important consequences of this combustion process on engine operation are the following:

1. Since injection commences just before combustion starts, there is no knock limit as in the spark-ignition engine resulting from spontaneous ignition of the premixed fuel and air in the end-gas. Hence a higher engine compression ratio can be used in the compression-ignition engine, improving its fuel conversion efficiency relative to the SI engine.
2. Since injection timing is used to control combustion timing, the delay period between the start of injection and start of combustion must be kept short (and reproducible). A short delay is also needed to hold the maximum cylinder gas pressure below the maximum the engine can tolerate. Thus, the spontaneous ignition characteristics of the fuel-air mixture must be held within a specified range. This is done by requiring that diesel fuel have a cetane number (a measure of the ease of ignition of that fuel in a typical diesel environment; see Sec. 10.6.2) above a certain value.
3. Since engine torque is varied by varying the amount of fuel injected per cycle with the engine air flow essentially unchanged, the engine can be operated unthrottled. Thus, pumping work requirements are low, improving part-load mechanical efficiency relative to the SI engine.
4. As the amount of fuel injected per cycle is increased, problems with air utilization during combustion lead to the formation of excessive amounts of soot which cannot be burned up prior to exhaust. This excessive soot or black smoke in the exhaust constrains the fuel/air ratio at maximum engine power to values 20 percent (or more) lean of stoichiometric. Hence, the maximum indicated mean effective pressure (in a naturally aspirated engine) is lower than values for an equivalent spark-ignition engine.
5. Because the diesel always operates with lean fuel/air ratios (and at part load with very lean fuel/air ratios), the effective value of $\gamma$ ($=c_p/c_v$) over the expansion process is higher than in a spark-ignition engine. This gives a higher fuel conversion efficiency than the spark-ignition engine, for a given expansion ratio (see Sec. 5.5.3).

The major problem in diesel combustion chamber design is achieving sufficiently rapid mixing between the injected fuel and the air in the cylinder to complete combustion in the appropriate crank angle interval close to top-center. The foregoing discussion indicates (and more detailed analysis will confirm) that mixing rates control the fuel burning rate. Commercial diesel engines are made with a very large range of cylinder sizes, with cylinder bores varying from about 70 to 900 mm. The mean piston speed at maximum rated power is approximately constant over this size range (see Sec. 2.2), so the maximum rated *engine* speed will be inversely proportional to the stroke [see Eq. (2.9)]. For a fixed crank angle interval for combustion (of order 40 to 50° to maintain high fuel conversion efficiency), the time available for combustion will, therefore, scale with the stroke. Thus, at the small end of the diesel engine size range, the mixing between the injected fuel and the air must take place on a time scale some 10 times shorter than in engines at the large end of this range. It would be expected, therefore, that the design of the engine combustion chamber (including the inlet port and valve) and the fuel-injection system would have to change substantially over this size range to provide the fuel and air motion inside the cylinder required to achieve the desired fuel-air mixing rate. As engine size decreases, more vigorous air motion is required while less fuel jet penetration is necessary. It is this logic, primarily, that leads to the different diesel combustion chamber designs and fuel injection systems found in practice over the large size range of commercial diesel engines.



## 10.2 TYPES OF DIESEL COMBUSTION SYSTEMS

Diesel engines are divided into two basic categories according to their combustion chamber design: (1) *direct-injection (DI) engines*, which have a single open combustion chamber into which fuel is injected directly; (2) *indirect-injection (IDI) engines*, where the chamber is divided into two regions and the fuel is injected into the "prechamber" which is connected to the main chamber (situated above the piston crown) via a nozzle, or one or more orifices. IDI engine designs are only used in the smallest engine sizes. Within each category there are several different chamber geometry, air-flow, and fuel-injection arrangements.

### 10.2.1 Direct-Injection Systems

In the largest-size engines, where mixing rate requirements are least stringent, quiescent direct-injection systems of the type shown in Fig. 10-1a are used. The momentum and energy of the injected fuel jets are sufficient to achieve adequate fuel distribution and rates of mixing with the air. Additional organized air motion is not required. The combustion chamber shape is usually a shallow bowl in the crown of the piston, and a central multihole injector is used.

As engine size decreases, increasing amounts of air swirl are used to achieve faster fuel-air mixing rates. Air swirl is generated by suitable design of the inlet port (see Sec. 8.3); the swirl rate can be increased as the piston approaches TC by forcing the air toward the cylinder axis, into a bowl-in-piston type of combustion

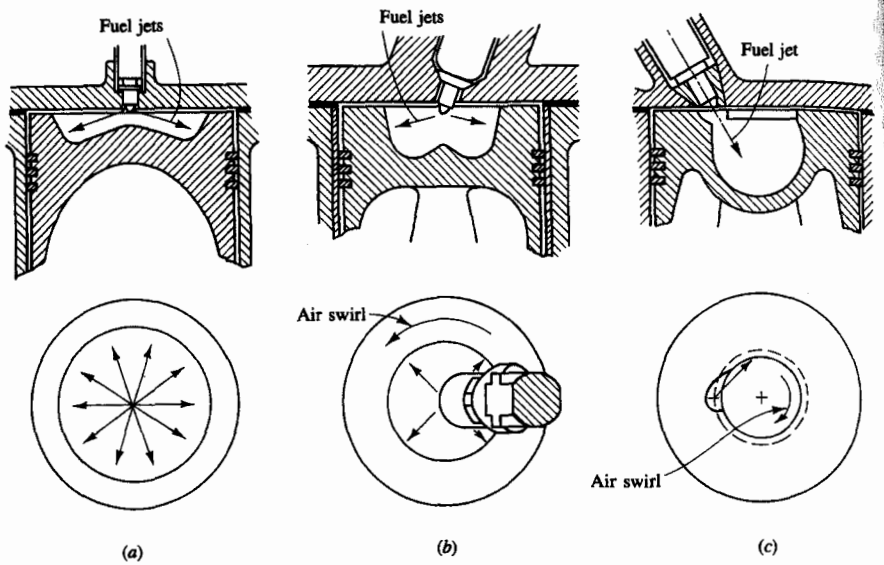


**FIGURE 10-1**
Common types of direct-injection compression-ignition or diesel engine combustion systems: (*a*) quiescent chamber with multihole nozzle typical of larger engines; (*b*) bowl-in-piston chamber with swirl and multihole nozzle; (*c*) bowl-in-piston chamber with swirl and single-hole nozzle. (*b*) and (*c*) used in medium to small DI engine size range.

chamber. Figure 10-1b and *c* shows the two types of DI engine with swirl in common use. Figure 10-1*b* shows a DI engine with swirl, with a centrally located multihole injector nozzle. Here the design goal is to hold the amount of liquid fuel which impinges on the piston cup walls to a minimum. Figure 10-1*c* shows the M.A.N. "M system" with its single-hole fuel-injection nozzle, oriented so that most of the fuel is deposited on the piston bowl walls. These two types of designs are used in medium-size (10- to 15-cm bore) diesels and, with increased swirl, in small-size (8- to 10-cm bore) diesels.

### 10.2.2 Indirect-Injection Systems

Inlet generated air swirl, despite amplification in the piston cup, has not provided sufficiently high fuel-air mixing rates for small high-speed diesels such as those used in automobiles. Indirect-injection or divided-chamber engine systems have been used instead, where the vigorous charge motion required during fuel injection is generated during the compression stroke. Two broad classes of IDI systems can be defined: (1) swirl chamber systems and (2) prechamber systems, as illustrated in Fig. 10-2*a* and *b*, respectively. During compression, air is forced from the main chamber above the piston into the auxiliary chamber, through the nozzle or orifice (or set of orifices). Thus, toward the end of compression, a vigorous flow in the auxiliary chamber is set up; in swirl chamber systems the connecting passage and chamber are shaped so that this flow within the auxiliary chamber rotates rapidly.



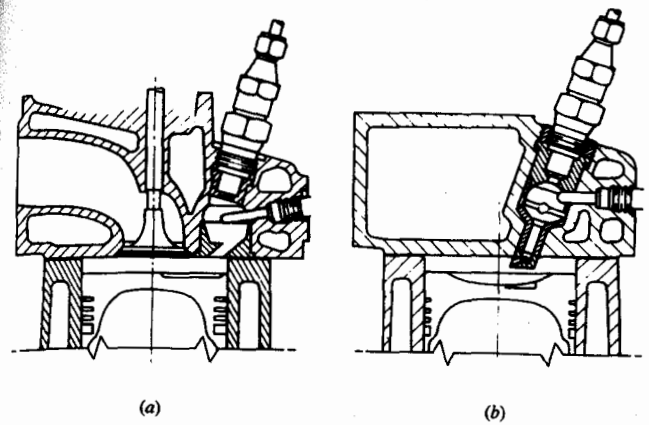


**FIGURE 10-2**
Two common types of small indirect-injection diesel engine combustion system: (*a*) swirl prechamber; (*b*) turbulent prechamber.

Fuel is usually injected into the auxiliary chamber at lower injection-system pressure than is typical of DI systems through a pintle nozzle as a single spray, as shown in Fig. 1-18. Combustion starts in the auxiliary chamber; the pressure rise associated with combustion forces fluid back into the main chamber where the jet issuing from the nozzle entrains and mixes with the main chamber air. The glow plug shown on the right of the prechamber in Fig. 10-2 is a cold-starting aid. The plug is heated prior to starting the engine to ensure ignition of fuel early in the engine cranking process.

### 10.2.3 Comparison of Different Combustion Systems

The number of different combustion chamber types proposed and tried since the beginnings of diesel engine development is substantial. Over the years, however, through the process of evolution and the increased understanding of the physical and chemical processes involved, only a few designs based on a sound principle have survived. The important characteristics of those chambers now most commonly used are summarized in Table 10.1. The numbers for dimensions and operating characteristics are typical ranges for each different type of diesel engine and combustion system.

The largest, slowest speed, engines for power generation or marine applications use open quiescent chambers which are essentially disc shaped; the motion of the fuel jets is responsible for distributing and mixing the fuel. These are usually two-stroke cycle engines. In the next size range, in large truck and locomotive engines, a quiescent chamber consisting of a shallow dish or bowl in the

TABLE 10.1
**Characteristics of Common Diesel Combustion Systems**

| | Direct injection | | | | Indirect injection | |
|---|---|---|---|---|---|---|
| System | Quiescent | Medium swirl | High swirl "M" | High swirl multispray | Swirl chamber | Pre-chamber |
| Size | Largest | Medium | Medium—smaller | Medium—small | Smallest | Smallest |
| Cycle | 2-/4-stroke | 4-stroke | 4-stroke | 4-stroke | 4-stroke | 4-stroke |
| Turbocharged/supercharged/naturally aspirated | TC/S | TC/NA | TC/NA | NA/TC | NA/TC | NA/TC |
| Maximum speed, rev/min | 120–2100 | 1800–3500 | 2500–5000 | 3500–4300 | 3600–4800 | 4500 |
| Bore, mm | 900–150 | 150–100 | 130–80 | 100–80 | 95–70 | 95–70 |
| Stroke/bore | 3.5–1.2 | 1.3–1.0 | 1.2–0.9 | 1.1–0.9 | 1.1–0.9 | 1.1–0.9 |
| Compression ratio | 12–15 | 15–16 | 16–18 | 16–22 | 20–24 | 22–24 |
| Chamber | Open or shallow dish | Bowl-in-piston | Deep bowl-in-piston | Deep bowl-in-piston | Swirl pre-chamber | Single/multi-orifice pre-chamber |
| Air-flow pattern | Quiescent | Medium swirl | High swirl | Highest swirl | Very high swirl in pre-chamber | Very turbulent in pre-chamber |
| Number of nozzle holes | Multi | Multi | Single | Multi | Single | Single |
| Injection pressure | Very high | High | Medium | High | Lowest | Lowest |

piston crown is often used. The air utilization in these engines is low, but they are invariably supercharged or turbocharged to obtain high power density.

In the DI category, as engine size decreases and maximum speed rises, swirl is used increasingly to obtain high-enough fuel-air mixing rates. The swirl is generated by suitably shaped inlet ports, and is amplified during compression by forcing most of the air toward the cylinder axis into the deep bowl-in-piston combustion chamber. In about the same size range, an alternative system to the multihole nozzle swirl system is the M.A.N. "M" system (or wall-wetting system), where most of the fuel from the single-hole pintle nozzle is placed on the wall of the spherical bowl in the piston crown.

In the smallest engine sizes, the IDI engine has traditionally been used to obtain the vigorous air motion required for high fuel-air mixing rates. There are several different geometries in use. These either generate substantial swirl in the auxiliary chamber during the latter part of the compression stroke, using a nozzle or connecting passage that enters the auxiliary chamber tangentially, or they generate intense turbulence in the prechamber through use of several small orifices and obstructions to the flow within the prechamber. The most common design of swirl chamber is the Ricardo Comet design shown in Fig. 10-2*a*. An alternative IDI engine to the two types listed in Table 10-1 is the air cell system. In that system the fuel is injected into the main chamber and not the auxiliary "air cell." The auxiliary chamber acts as a turbulence generator as gas flows into and out of the cell.



## 10.3 PHENOMENOLOGICAL MODEL OF COMPRESSION-IGNITION ENGINE COMBUSTION

Studies of photographs of diesel engine combustion, combined with analyses of engine cylinder pressure data, have led to a widely accepted descriptive model of the compression-ignition engine combustion process. The concept of *heat-release rate* is important to understanding this model. It is defined as the rate at which the chemical energy of the fuel is released by the combustion process. It can be calculated from cylinder pressure versus crank angle data, as the energy release required to create the measured pressure, using the techniques described in Sec. 10.4. The combustion model defines four separate phases of diesel combustion, each phase being controlled by different physical or chemical processes. Although the relative importance of each phase does depend on the combustion system used, and engine operating conditions, these four phases are common to all diesel engines.

### 10.3.1 Photographic Studies of Engine Combustion

High-speed photography at several thousand frames per second has been used extensively to study diesel engine combustion. Some of these studies have been carried out in combustion chambers very close to those used in practice, under normal engine operating conditions (e.g., Refs. 1 and 2). Sequences of individual frames from movies provide valuable information on the nature of the combustion process in the different types of diesel engines. Figure 10-3 shows four combustion chamber geometries that have been studied photographically. These are: (*a*) a quiescent chamber typical of diesel engines in the 3 to 20 $dm^3$/cylinder displacement used for industrial, marine, and rail traction applications (only the burning of a single fuel spray of the multispray combustion system could be studied[2]); (*b*) a smaller high-speed DI engine with swirl and four fuel jets centrally injected; (*c*) an M.A.N. "M" DI system; and (*d*) a Ricardo Comet V swirl chamber IDI system.[1]

The combustion sequences were recorded on color film and show the following features:

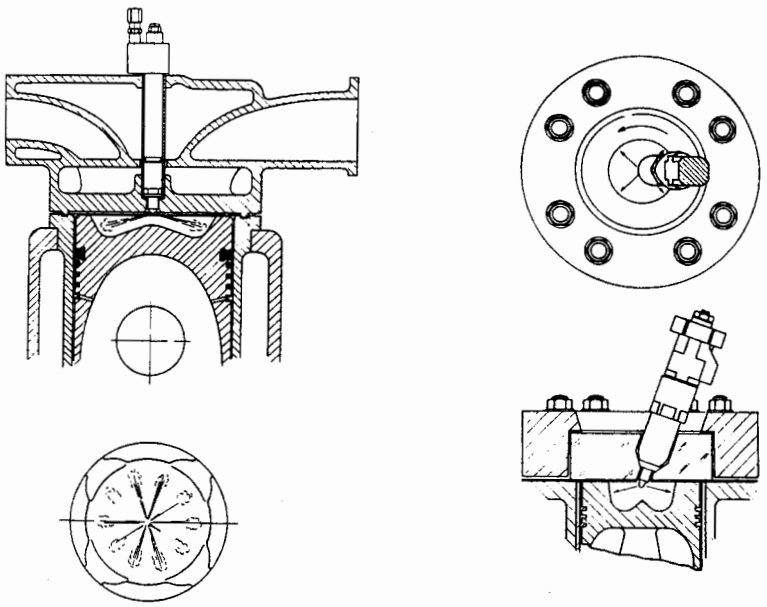

(*a*) (*b*)

**FIGURE 10-3**
Four diesel combustion chambers used to obtain photographs of the compression-ignition combustion process shown in Fig. 10-4 on color plate: (*a*) quiescent DI chamber; (*b*) multihole nozzle DI chamber with swirl: on p. 499; (*c*) M.A.N. "M" DI chamber; (*d*) Ricardo Comet IDI swirl chamber.[1,2]

*Fuel spray(s).* The fuel droplets reflect light from spot lamps and define the extent of the liquid fuel spray prior to complete vaporization.

*Premixed flame.* These regions are of too low a luminosity to be recorded with the exposure level used. The addition of a copper additive dope to the fuel gives these normally blue flames a green color bright enough to render them visible.

*Diffusion flame.* The burning high-temperature carbon particles in this flame provide more than adequate luminosity and appear as yellow-white. As the flame cools, the radiation from the particles changes color through orange to red.

*Over-rich mixture.* The appearance of a brown region, usually surrounded by a white diffusion flame, indicates an excessively rich mixture region where substantial soot particle production has occurred. Where this fuel-rich soot-laden cloud contacts unburned air there is a hot white diffusion flame.

Table 10.2 summarizes the characteristics of these different regions, discernable in the photographs shown in Fig. 10-4 on the color plate.

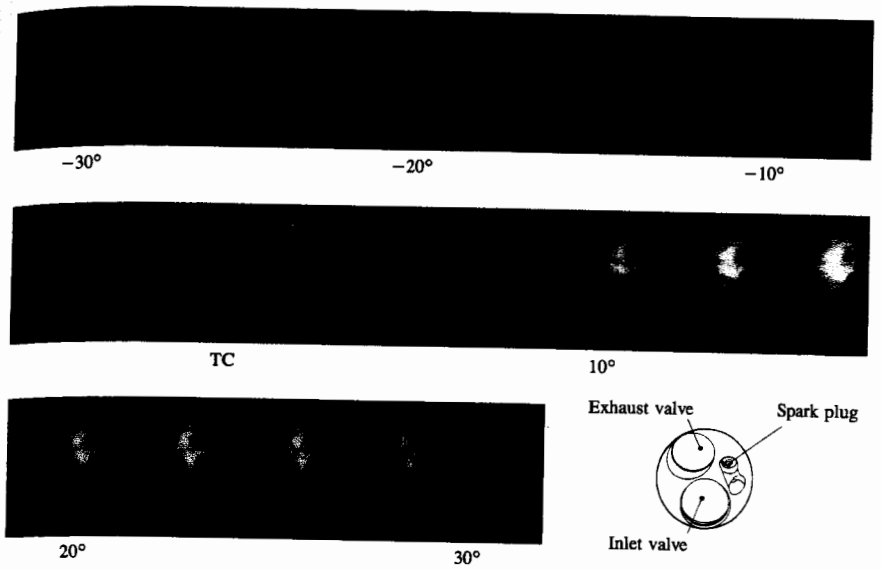


**FIGURE 9-1**

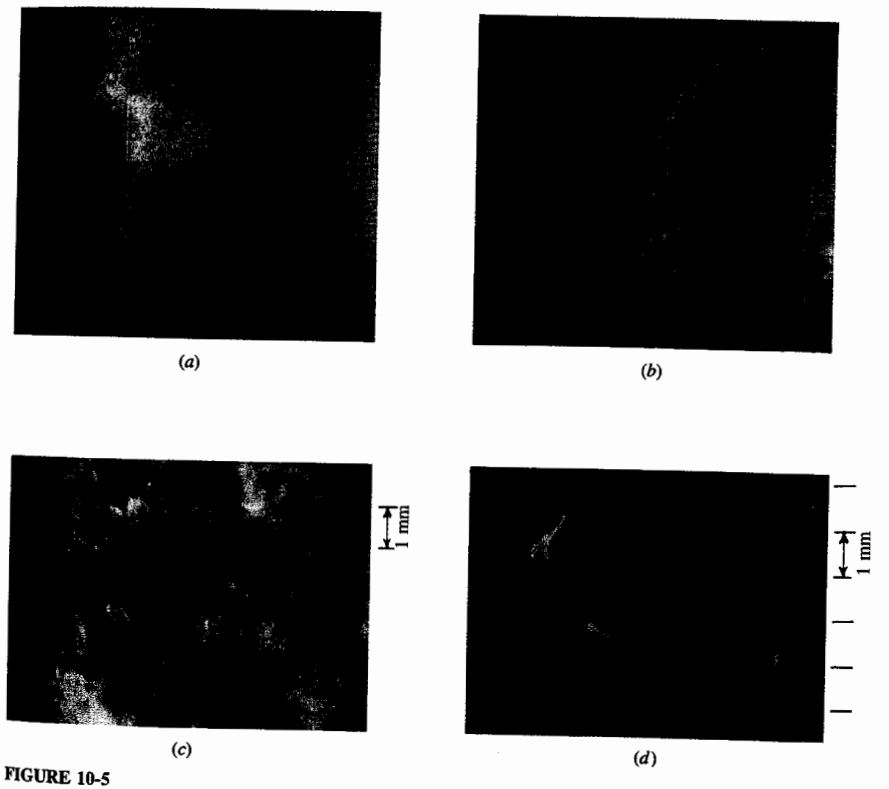


(*a*) (*b*) (*c*) (*d*)

**FIGURE 10-5**

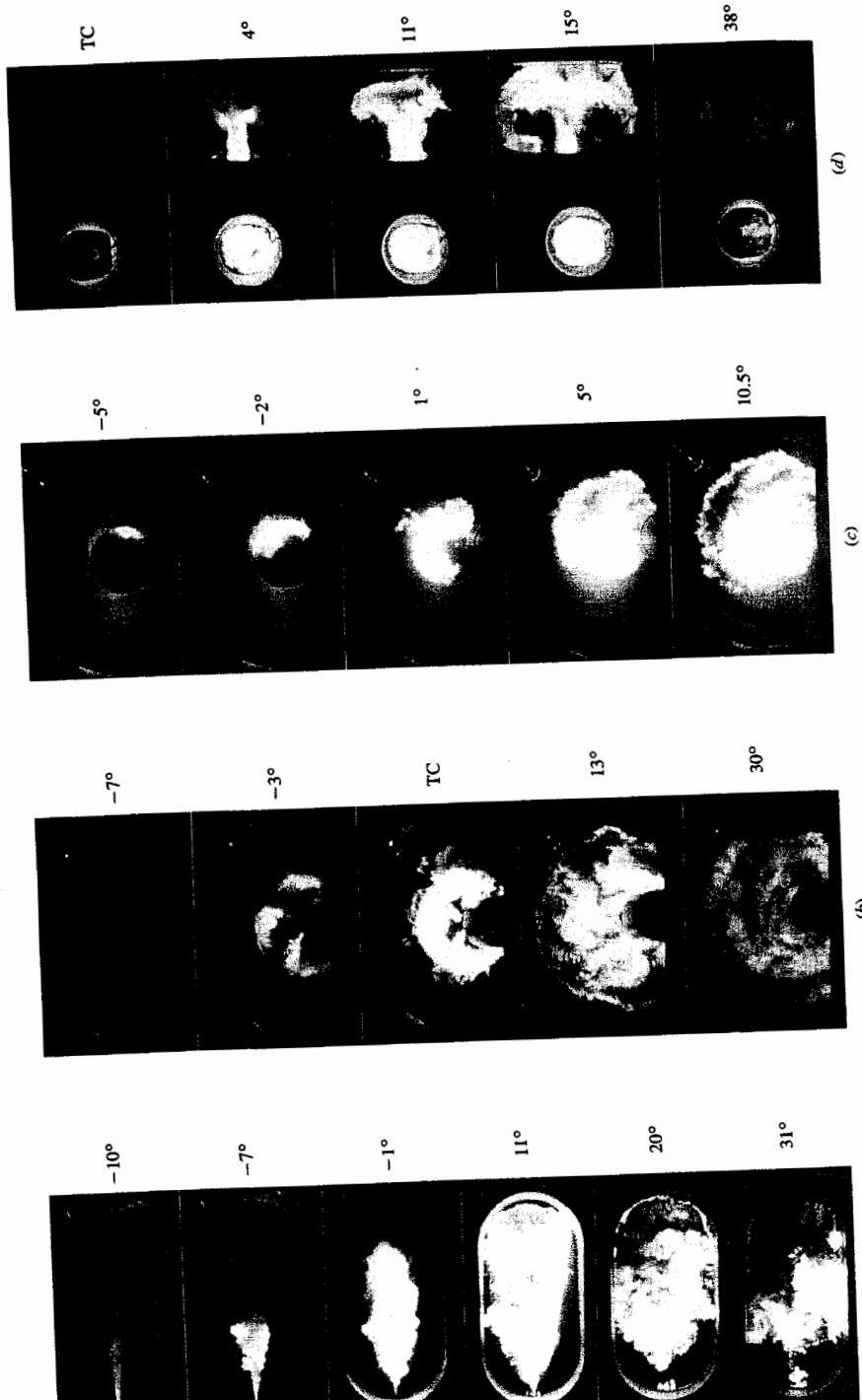


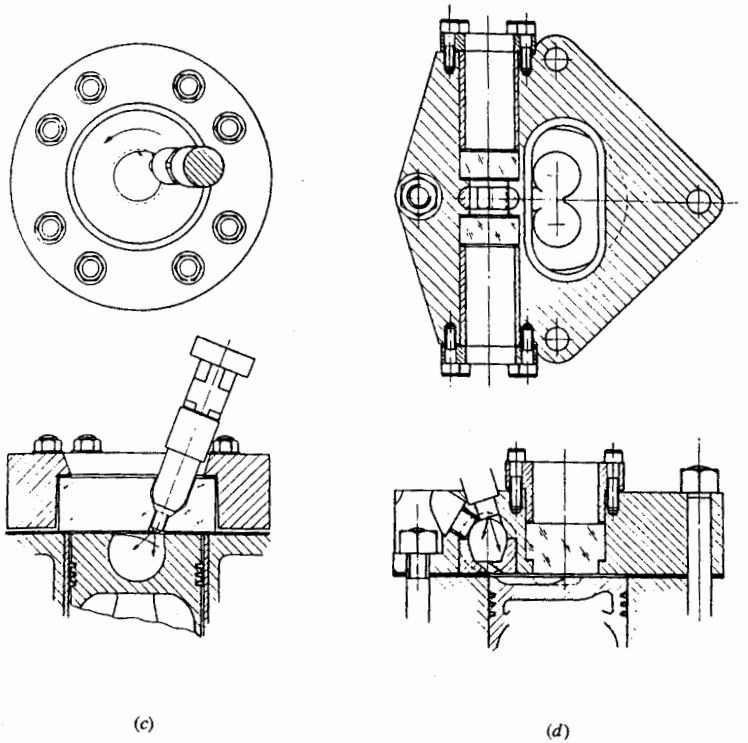


Figure 10-4*a* shows a sequence of photographs from one combustion event of the single spray, burning under conditions typical of a large quiescent DI engine. The fuel spray is shown penetrating into the chamber. Ignition occurs at −8° in the fuel-air mixture left behind on the edge of the spray not far from the injector. The flame then spreads rapidly (−7°) along the outside of the spray to the spray tip. Here some of the fuel, which has had a long residence time in the chamber, burns with a blue-green low-luminosity flame (colored green by the copper fuel additive). The flame engulfing the remainder of the spray is brilliant white-yellow from the burning of the soot particles which have been formed in

**FIGURE 10-4 (On Color Plate, facing this page)**
Sequence of photographs from high-speed movies taken in special visualization diesel engines shown in Fig. 10-3: (*a*) combustion of single spray burning under large DI engine conditions; (*b*) combustion of four sprays in DI engine with counterclockwise swirl; (*c*) combustion of single spray in M.A.N. "M" DI diesel; (*d*) combustion in prechamber (on left) and main chamber (on right) in Ricardo Comet IDI swirl chamber diesel. 1250 rev/min, imep = 827 kPa (120 lb/in$^2$)[1, 2] (*Courtesy Ricardo Consulting Engineers.*)

**TABLE 10.2**
**Interpretation of diesel engine combustion color photographs[1]**

| Color | Interpretation |
|---|---|
| Grey | Background; the gas (air in early stages, combustion products later) is transparent and not glowing |
| Green | Early in combustion process; low luminosity "premixed"-type flame, rendered visible by copper added to fuel. Later; burned gas above about 1800°C |
| White, and yellow-white | Carbon particle burnup in diffusion flame, 2000–2500°C |
| Yellow, orange-red | Carbon burnup in diffusion flame at lower temperatures; last visible in film at 1000°C |
| Brown | Soot clouds from very fuel-rich mixture regions. Where these meet air (grey) there is always a white fringe of hot flame |

the fuel-rich spray core. At this stage (−1°), about 60 percent of the fuel has been injected. The remainder is injected into this enflamed region, producing a very fuel-rich zone apparent as the dark brown cloud (11°). This soot cloud moves to the outer region of the chamber (11° to 20°); white-yellow flame activity continues near the injector, probably due to combustion of ligaments of fuel which issued from the injector nozzle as the injector needle was seating. Combustion continues well into the expansion stroke (31°C).

This sequence shows that fuel distribution is always highly nonuniform during the combustion process in this type of DI engine. Also the air which is between the individual fuel sprays of the quiescent open-chamber diesel mixes with each burning spray relatively slowly, contributing to the poor air utilization with this type of combustion chamber.

Figure 10-4*b* shows a combustion sequence from the DI engine with swirl (the chamber shown in Fig. 10-3*b*). The inner circle corresponds to the deep bowl in the piston crown, the outer circle to the cylinder liner. The fuel sprays (of which two are visible without obstruction from the injector) first appear at −13°. At −7° they have reached the wall of the bowl; the tips of the sprays have been deflected slightly by the anticlockwise swirl. The frame at −3° shows the first ignition. Bright luminous flame zones are visible, one on each spray. Out by the bowl walls, where fuel vapor has been blown around by the swirl, larger greenish burning regions indicating the presence of premixed flame can be seen. The fuel downstream of each spray is next to ignite, burning yellow-white due to the soot



formed by the richer mixture. Flame propagation back to the injector follows extremely rapidly and at TC the bowl is filled with flame. At 5° ATC the flame spreads out over the piston crown toward the cylinder wall due to combustion-produced gas expansion and the reverse squish flow (see Sec. 8.4). The brown regions (13°) are soot-laden fuel-rich mixture originating from the fuel which impinges on the wall. The last frame (30° ATC) shows the gradual diminution of the soot-particle-laden regions as they mix with the excess air and burn up. The last dull-red flame visible on the film is at about 75° ATC, well into the expansion stroke.

Figure 10-4*c* shows the combustion sequence for the M.A.N. "M"-type DI engine. In the version of the system used for these experiments, the fuel was injected through a two-hole nozzle which produces a main jet directed tangentially onto the walls of the spherical cup in the piston crown, and an auxiliary spray which mixes a small fraction of the fuel directly with the swirling air flow. More recent "M" systems use a pintle nozzle with a single variable orifice.[3] At −5° the fuel spray is about halfway round the bowl. Ignition has just occurred of fuel adjacent to the wall which has mixed sufficiently with air to burn. The flame spreads rapidly (−2°, 1°) to envelop the fuel spray, and is convected round the cup by the high swirl air flow. By shortly after TC the flame has filled the bowl and is spreading out over the piston crown. A soot cloud is seen near the top right of the picture at 5° ATC which spreads out around the circumference of the enflamed region. There is always a rim of flame between the soot cloud and the cylinder liner as excess air is mixed into the flame zone (10.5°). The flame is of the carbon-burning type throughout; little premixed green flame is seen even at the beginning of the combustion process.

Figure 10-4*d* shows the combustion sequence in a swirl chamber IDI engine of the Ricardo Comet V design. The swirl chamber (on the left) is seen in the view of the lower drawing of Fig. 10-3*d* (with the connecting passageway entering the swirl chamber tangentially at the bottom left to produce clockwise swirl). The main chamber is seen in the plan view of the upper drawing of Fig. 10-3*d*. Two sprays emerge from the Pintaux nozzle after the start of injection at −11°. The smaller auxiliary spray which is radial is sharply deflected by the high swirl. Frame 1 shows how the main spray follows the contour of the chamber; the auxiliary spray has evaporated and can no longer be seen. The first flame occurs at −1° in the vaporized fuel from the auxiliary spray and is a green premixed flame. The flame then spreads to the main spray (TC), becoming a yellow-white carbon-particle-burning flame with a green fringe. At 4° ATC the swirl chamber appears full of carbon-burning flame, which is being blown down the throat and into the recesses in the piston crown by the combustion generated pressure rise in the prechamber. The flame jet impinges on the piston recesses entraining the air in the main chamber, leaving green patches where all carbon is burned out (4°, 11°, 15°). A brown soot cloud is emerging from the throat. By 15° ATC this soot cloud has spread around the cylinder, with a bright yellow-white flame at its periphery. This soot then finds excess air and burns up, while the yellow-white

flame becomes yellow and then orange-red as the gases cool on expansion. By 38° ATC most of the flame is burnt out.

Magnified color photographs of the flame around a single fuel spray under conditions typical of a direct-injection diesel engine, shown in Fig. 10-5 on the color plate, provide additional insight into the compression-ignition and flame-development processes.[4] These photographs were obtained in a rapid compression machine: this device is a cylinder-piston apparatus in which air is rapidly compressed by moving the piston to temperatures and pressures similar to those in the diesel engine combustion chamber at the time of injection. A single fuel spray was then injected into the disc-shaped combustion chamber. The air flow prior to compression was forced to swirl around the cylinder axis and much of that swirl remains after compression.

Figure 10-5*a* shows a portion of the liquid fuel spray (which appears black due to back lighting) and the rapidly developing flame 0.4 ms after ignition occurs. Ignition commences in the *fuel vapor*–air mixture region, set up by the jet motion and swirling air flow, away from the liquid core of the spray. In this region the smaller fuel droplets have evaporated in the hot air atmosphere that surrounds them and mixed with sufficient air for combustion to occur. Notice that the fuel vapor concentration must be nonuniform; combustion apparently occurs around small "lumps" of mixture of the appropriate composition and temperature. Figure 10-5*b* shows the same flame at a later time, 3.2 ms after ignition. The flame now surrounds most of the liquid spray core. Its irregular boundary reflects the turbulent character of the fuel spray and its color variation indicates that the temperature and composition in the flame region are not uniform.

Figure 10-5*c* shows a portion of this main flame region enlarged to show its internal structure. A highly convoluted flame region is evident, which has a similar appearance to a gaseous turbulent diffusion flame. The major portion of the diesel engine flame has this character, indicative of the burning of fuel vapor–air pockets or lumps or eddies of the appropriate composition. Only at the end of the combustion process is there visible evidence of individual fuel droplets burning with an envelope flame. Figure 10-5*d* shows the same region of the combustion chamber as Fig. 10-5*c*, but at the end of the burning process well after injection has been completed. A few large droplets are seen burning with individual droplet flames. It is presumed that such large drops were formed at the end of the injection process as the injector nozzle was closing.

**FIGURE 10-5 (On Color Plate, facing page 498)**
Photographs from high-speed movie of single fuel spray injected into a swirling air flow in a rapid-compression machine. (*a*) Spray and flame 0.4 ms after ignition; scale on right in millimeters. (*b*) Flame surrounding spray 3.2 ms after ignition. (*c*) Magnified photograph of main portion of flame. (*d*) Individual droplet burning late in combustion process after injection completed. Air temperature ~500°C. 50 mg fuel injected.[4] (*Courtesy Professor M. Ogasawara, Osaka University.*)



### 10.3.2 Combustion in Direct-Injection, Multispray Systems

Figure 10-6 shows typical data for cylinder pressure ($p$), fuel-injector needle-lift, and fuel pressure in the nozzle gallery through the compression and expansion strokes of a direct-injection diesel. The engine had central fuel injection through a four-hole nozzle into a disc-shaped bowl-in-piston combustion chamber. The rate of fuel injection can be obtained from the fuel-line pressure, cylinder pressure, nozzle geometry, and needle-lift profiles by considering the injector as one or more flow restrictions;[5] it is similar in phasing and comparable in shape to the needle-lift profile. There is a delay of 9° between the start of injection and start of combustion [identified by the change in slope of the $p(\theta)$ curve]. The pressure rises rapidly for a few crank angle degrees, then more slowly to a peak value about 5° after TC. Injection continues after the start of combustion. A rate-of-heat-release diagram† from the same study, corresponding to this rate of fuel injection and cylinder pressure data, is shown in Fig. 10-7. The general shape of the rate-of-heat-release curve is typical of this type of DI engine over its load and speed range. The heat-release-rate diagram shows negligible heat release until toward the end of compression when a slight loss of heat during the delay period (which is due to heat transfer to the walls and to fuel vaporization and heating) is

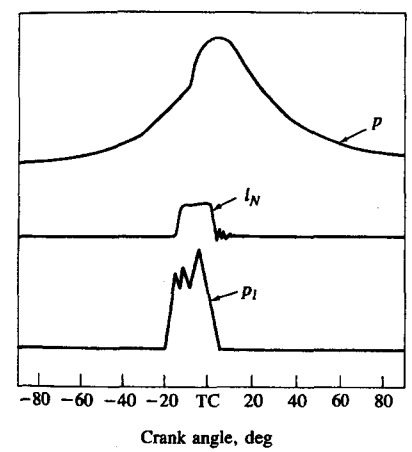


**FIGURE 10-6**
Cylinder pressure $p$, injector needle lift $l_N$, and injection-system fuel-line pressure $p_l$, as functions of crank angle for small DI diesel engine.[5]

† The heat-release rate plotted here is the net heat-release rate (see Sec. 10.4). It is the sum of the change of sensible internal energy of the cylinder gases and the work done on the piston. It differs from the rate of fuel energy released by combustion by the heat transferred to the combustion chamber walls. The heat loss to the walls is 10 to 25 percent of the fuel heating value in smaller engines; it is less in larger engine sizes. This net heat release can be used as an indicator of actual heat release when the heat loss is small.

evident. During the combustion process the burning proceeds in three distinguishable stages. In the first stage, the rate of burning is generally very high and lasts for only a few crank angle degrees. It corresponds to the period of rapid cylinder pressure rise. The second stage corresponds to a period of gradually decreasing heat-release rate (though it initially may rise to a second, lower, peak as in Fig. 10-7). This is the main heat-release period and lasts about 40°. Normally about 80 percent of the total fuel energy is released in the first two periods. The third stage corresponds to the "tail" of the heat-release diagram in which a small but distinguishable rate of heat release persists throughout much of the expansion stroke. The heat release during this period usually amounts to about 20 percent of the total fuel energy.

From studies of rate-of-injection and heat-release diagrams such as those in Fig. 10-7, over a range of engine loads, speeds, and injection timings, Lyn[6] developed the following summary observations. First, the total burning period is much longer than the injection period. Second, the absolute burning rate increases proportionally with increasing engine speed; thus on a crank angle basis, the burning interval remains essentially constant. Third, the magnitude of the initial peak of the burning-rate diagram depends on the ignition delay period, being higher for longer delays. These considerations, coupled with engine combustion photographic studies, lead to the following model for diesel combustion.

Figure 10-8 shows schematically the rate-of-injection and rate-of-burning diagrams, where the injected fuel as it enters the combustion chamber has been divided into a number of elements. The first element which enters mixes with air and becomes "ready for burning" (i.e., mixes to within combustible limits), as shown conceptually by the lowest triangle along the abscissa in the rate-of-burning figure. While some of this fuel mixes rapidly with air, part of it will mix much more slowly. The second and subsequent elements will mix with air in a similar manner, and the total "ready-for-burning" diagram, enclosed by the dashed line, is obtained. The total area of this diagram is equal to that of the rate-of-injection diagram. Ignition does not occur until after the delay period is over, however. At the ignition point, some of the fuel already injected has mixed with enough air to be within the combustible limits. That "premixed" fuel-air

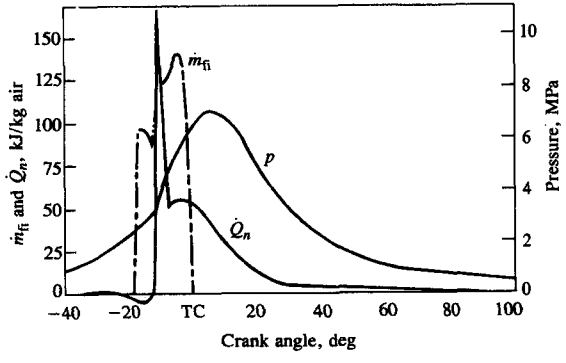


**FIGURE 10-7**
Cylinder pressure $p$, rate of fuel injection $\dot{m}_{fi}$, and net heat-release rate $\dot{Q}_n$ calculated from $p$ for small DI diesel engine, 1000 rev/min, normal injection timing, bmep = 620 kPa.[5]



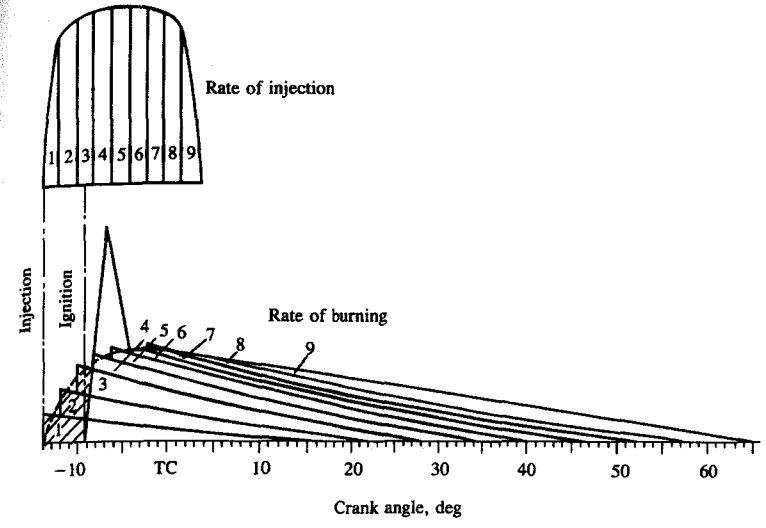


**FIGURE 10-8**
Schematic of relationship between rate of fuel injection and rate of fuel burning or energy release.[6]

mixture (the shaded region in Fig. 10-8) is then added to the mixture which becomes ready for burning after the end of the delay period, producing the high initial rate of burning as shown. Such a heat-release profile is generally observed with this type of naturally aspirated DI diesel engine. Photographs (such as those in Fig. 10-4*a* and *b*) show that up to the heat-release-rate peak, flame regions of low green luminosity are apparent because the burning is predominantly of the premixed part of the spray. After the peak, as the amount of premixed mixture available for burning decreases and the amount of fresh mixture mixed to be "ready for burning" increases, the spray burns essentially as a turbulent diffusion flame with high yellow-white or orange luminosity due to the presence of carbon particles.

To summarize, the following stages of the overall compression-ignition diesel combustion process can be defined. They are identified on the typical heat-release-rate diagram for a DI engine in Fig. 10-9.

*Ignition delay* (*ab*). The period between the start of fuel injection into the combustion chamber and the start of combustion [determined from the change in slope on the $p$-$\theta$ diagram, or from a heat-release analysis of the $p(\theta)$ data, or from a luminosity detector].

*Premixed or rapid combustion phase* (*bc*). In this phase, combustion of the fuel which has mixed with air to within the flammability limits during the ignition delay period occurs rapidly in a few crank angle degrees. When this burning mixture is added to the fuel which becomes ready for burning and burns during this phase, the high heat-release rates characteristic of this phase result.

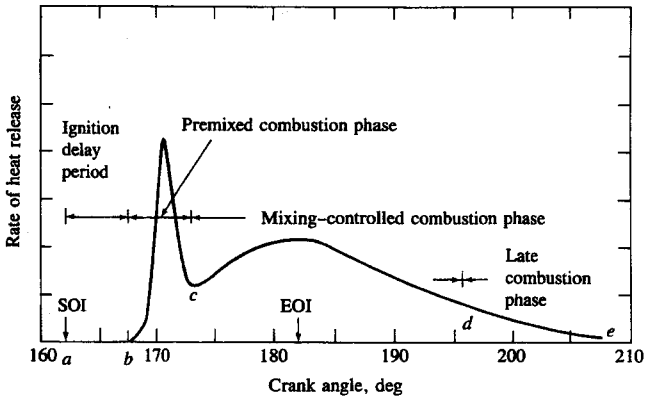


**FIGURE 10-9**
Typical DI engine heat-release-rate diagram identifying different diesel combustion phases.

*Mixing-controlled combustion phase* (*cd*). Once the fuel and air which premixed during the ignition delay have been consumed, the burning rate (or heat-release rate) is controlled by the rate at which mixture becomes available for burning. While several processes are involved—liquid fuel atomization, vaporization, mixing of fuel vapor with air, preflame chemical reactions—the rate of burning is controlled in this phase primarily by the fuel vapor–air mixing process. The heat-release rate may or may not reach a second (usually lower) peak in this phase; it decreases as this phase progresses.

*Late combustion phase* (*de*). Heat release continues at a lower rate well into the expansion stroke. There are several reasons for this. A small fraction of the fuel may not yet have burned. A fraction of the fuel energy is present in soot and fuel-rich combustion products and can still be released. The cylinder charge is nonuniform and mixing during this period promotes more complete combustion and less-dissociated product gases. The kinetics of the final burnout processes become slower as the temperature of the cylinder gases fall during expansion.

### 10.3.3 Application of Model to Other Combustion Systems

In the M.A.N. "M" DI engine system, and in IDI systems, the shapes of the heat-release-rate curve are different from those of the quiescent or moderate swirl DI shown in Figs. 10-7 and 10-9. With the "M" system, the initial heat-release "spike" is much less pronounced (in spite of the fact that a large fraction of the fuel is injected during the delay period) though the total burning period is about the same. Lyn[6] has suggested that the lower initial burning rate is due to the fact that the smaller number of nozzle holes (one or two instead of about four or more) and the directing of the main spray tangentially to the wall substantially reduce the free mixing surface area of the fuel jets. However, since the burning



rates after ignition are relatively high, mixing must speed up. This occurs due to the centrifugal forces set up in the swirling flow. Initially, the fuel is placed near the wall, and mixing is inhibited by the effect of the high centrifugal forces on the fuel vapor which is of higher density than the air and so tends to remain near the wall. Once ignition occurs, the hot burning mixture expands, decreases in density, and is then moved rapidly toward the center of the chamber. This strong radial mixing is the rate-determining process. An additional delaying mechanism exists if significant fuel is deposited on the wall. At compression air temperatures, the heat transferred to the fuel film on the wall from the gases in the cylinder is too small to account for the observed burning rates. Only after combustion starts will the gas temperature and heat-transfer rates be high enough to evaporate the fuel off the wall at an adequate rate.

In the swirl chamber IDI engine, where the air in the main chamber is not immediately available for mixing, again the rate-determining processes are different.[6] There is no initial spike on the rate-of-heat-release curve as was the case with DI engines. The small size of the chamber, together with the high swirl rate generated just before injection, results in considerable fuel impingement on the walls. This and the fact that the ignition delay is usually shorter with the IDI engine due to the higher compression ratio used account for the low initial burning rate.

Based on the above discussion Lyn[6] proposed three basic injection, mixing, and burning patterns important in diesel engines:

A. Fuel injection across the chamber with substantial momentum. Mixing proceeds immediately as fuel enters the chamber and is little affected by combustion.

B. Fuel deposition on the combustion chamber walls. Negligible mixing during the delay period due to limited evaporation. After ignition, evaporation becomes rapid and its rate is controlled by access of hot gases to the surface, radial mixing being induced by differential centrifugal forces. Burning is therefore delayed by the ignition lag.

C. Fuel distributed near the wall: mixing proceeds during the delay, but at a rate smaller than in mechanism A. After ignition, mixing is accelerated by the same mechanism as in mechanism B.

Figure 10-10 shows, schematically, the construction of the burning-rate or heat-release-rate diagrams (from the same injection-rate diagram) for the DI diesel combustion system with a central multihole nozzle, for the "M"-type DI diesel, and for the swirl chamber IDI. For the DI engine with multihole nozzle, mechanism A is predominant. For the DI engine with fuel sprayed tangentially to the wall, mechanisms B and C prevail; the delayed mixing prevents excessively high initial burning rates. For the IDI swirl chamber engine, the shorter ignition delay together with mixing process C during the delay period produces a gradual increase in burning rate, as shown in Fig. 10-10*c*.

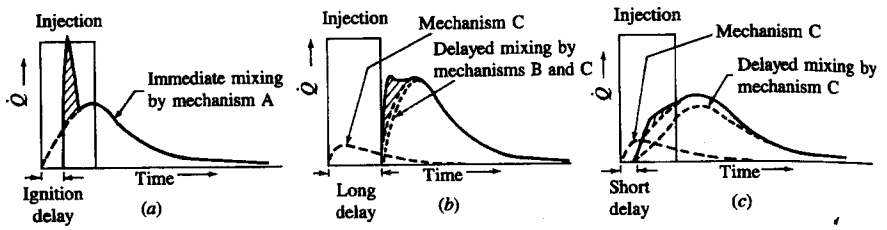


**FIGURE 10-10**
Schematic injection-rate and burning-rate diagrams in three different types of naturally aspirated diesel combustion system: (*a*) DI engine with central multihole nozzle; (*b*) DI "M"-type engine with fuel injected on wall; (*c*) IDI swirl chamber engine. Mechanisms A, B, and C defined in text.[6]

## 10.4 ANALYSIS OF CYLINDER PRESSURE DATA

Cylinder pressure versus crank angle data over the compression and expansion strokes of the engine operating cycle can be used to obtain quantitative information on the progress of combustion. Suitable methods of analysis which yield the rate of release of the fuel's chemical energy (often called heat release), or rate of fuel burning, through the diesel engine combustion process will now be described. The methods of analysis are similar to those described in Sec. 9.2.2 for spark-ignition engines and start with the first law of thermodynamics for an open system which is quasi static (i.e., uniform in pressure and temperature). The first law for such a system (see Fig. 9-11) is

$$\frac{dQ}{dt} - p\frac{dV}{dt} + \sum_i \dot{m}_i h_i = \frac{dU}{dt} \tag{10.1}$$

where $dQ/dt$ is the heat-transfer rate across the system boundary into the system, $p(dV/dt)$ is the rate of work transfer done by the system due to system boundary displacement, $\dot{m}_i$ is the mass flow rate into the system across the system boundary at location $i$ (flow out of the system would be negative), $h_i$ is the enthalpy of flux $i$ entering or leaving the system, and $U$ is the energy of the material contained inside the system boundary.

The following problems make the application of this equation to diesel combustion difficult:

1. Fuel is injected into the cylinder. Liquid fuel is added to the cylinder which vaporizes and mixes with air to produce a fuel/air ratio distribution which is nonuniform and varies with time. The process is not quasi static.
2. The composition of the burned gases (also nonuniform) is not known.
3. The accuracy of available correlations for predicting heat transfer in diesel engines is not well defined (see Chap. 12).
4. Crevice regions (such as the volumes between the piston, rings, and cylinder wall) constitute a few percent of the clearance volume. The gas in these regions is cooled to close to the wall temperature, increasing its density and, therefore,



the relative importance of these crevices. Thus crevices increase heat transfer and contain a nonnegligible fraction of the cylinder charge at conditions that are different from the rest of the combustion chamber.

Due to difficulties in dealing with these problems, both sophisticated methods of analysis and more simple methods give only approximate answers.

### 10.4.1 Combustion Efficiency

In both heat-release and fuel mass burned estimations, an important factor is the completeness of combustion. Air utilization in diesels is limited by the onset of black smoke in the exhaust. The smoke is soot particles which are mainly carbon. While smoke and other incomplete combustion products such as unburned hydrocarbons and carbon monoxide represent a combustion inefficiency, the magnitude of that inefficiency is small. At full load conditions, if only 0.5 percent of the fuel supplied is present in the exhaust as black smoke, the result would be unacceptable. Hydrocarbon emissions are the order of or less than 1 percent of the fuel. The fuel energy corresponding to the exhausted carbon monoxide is about 0.5 percent. Thus, the combustion inefficiency [Eq. (4.69)] is usually less than 2 percent; the combustion efficiency is usually greater than about 98 percent (see Fig. 3-9). While these emissions are important in terms of their air-pollution impact (see Chap. 11), from the point of view of energy conversion it is a good approximation to regard combustion and heat release as essentially complete.

### 10.4.2 Direct-Injection Engines

For this type of engine, the cylinder contents are a single open system. The only mass flows across the system boundary (while the intake and exhaust valves are closed) are the fuel and the crevice flow. An approach which incorporates the crevice flow has been described in Sec. 9.2.2; crevice flow effects will be omitted here. Equation (10.1) therefore becomes

$$\frac{dQ}{dt} - p\frac{dV}{dt} + \dot{m}_f h_f = \frac{dU}{dt} \tag{10.2}$$

Two common methods are used to obtain combustion information from pressure data using Eq. (10.2). In both approaches, the cylinder contents are assumed to be at a uniform temperature at each instant in time during the combustion process. One method yields fuel energy- or heat-release rate; the other method yields a fuel mass burning rate. The term *apparent* is often used to describe these quantities since both are approximations to the real quantities which cannot be determined exactly.

**HEAT-RELEASE ANALYSIS.** If $U$ and $h_f$ in Eq. (10.2) are taken to be the sensible internal energy of the cylinder contents and the sensible enthalpy of the injected

fuel, respectively,† then $dQ/dt$ becomes the difference between the chemical energy or heat released by combustion of the fuel (a positive quantity) and the heat transfer from the system (in engines, the heat transfer is from the system and by thermodynamic convention is a negative quantity). Since $h_{s,f} \approx 0$, Eq. (10.2) becomes

$$\frac{dQ_n}{dt} = \frac{dQ_{ch}}{dt} - \frac{dQ_{ht}}{dt} = p\frac{dV}{dt} + \frac{dU_s}{dt} \tag{10.3}$$

The apparent *net heat-release* rate, $dQ_n/dt$, which is the difference between the apparent *gross heat-release* rate $dQ_{ch}/dt$ and the heat-transfer rate to the walls $dQ_{ht}/dt$, equals the rate at which work is done on the piston plus the rate of change of sensible internal energy of the cylinder contents.

If we further assume that the contents of the cylinder can be modeled as an ideal gas, then Eq. (10.3) becomes

$$\frac{dQ_n}{dt} = p\frac{dV}{dt} + mc_v\frac{dT}{dt} \tag{10.4}$$

From the ideal gas law, $pV = mRT$, with $R$ assumed constant, it follows that

$$\frac{dp}{p} + \frac{dV}{V} = \frac{dT}{T} \tag{10.5}$$

Equation (10.5) can be used to eliminate $T$ from Eq. (10.4) to give

$$\frac{dQ_n}{dt} = \left(1 + \frac{c_v}{R}\right)p\frac{dV}{dt} + \frac{c_v}{R}V\frac{dp}{dt}$$

or

$$\frac{dQ_n}{dt} = \frac{\gamma}{\gamma - 1}p\frac{dV}{dt} + \frac{1}{\gamma - 1}V\frac{dp}{dt} \tag{10.6}$$

Here $\gamma$ is the ratio of specific heats, $c_p/c_v$. An appropriate range for $\gamma$ for diesel heat-release analysis is 1.3 to 1.35; Eq. (10.6) is often used with a constant value of $\gamma$ within this range. More specifically, we would expect $\gamma$ for diesel engine heat-release analysis to have values appropriate to air at end-of-compression-stroke temperatures prior to combustion ($\approx$1.35) and to burned gases at the overall equivalence ratio following combustion ($\approx$1.26–1.3). The appropriate values for $\gamma$ during combustion which will give most accurate heat-release information are not well defined.[7, 8]

More complete methods of heat-release analysis based on Eq. (10.2) have been proposed and used. These use more sophisticated models for the gas properties before, during, and after combustion, and for heat transfer and crevice effects.[8] However, it is also necessary to deal with the additional issues of: (1) mixture nonuniformity (fuel/air ratio nonuniformity *and* burned and unburned gas nonuniformities); (2) accuracy of any heat-transfer model used (see Chap. 12);

† That is, $U = U_s = U(T) - U(298\text{ K})$ and $h_f = h_{s,f} = h_f(T) - h_f(298\text{ K})$; see Sec. 5.5 for definition.



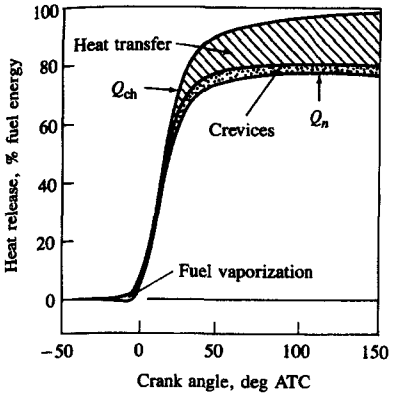


**FIGURE 10-11**
Gross and net heat-release profile during combustion, for a turbocharged DI diesel engine in mid-load, mid-speed range, showing relative magnitude of heat transfer, crevice, and fuel vaporization and heatup effects.

and (3) the effects of the crevice regions. These additional phenomena must be dealt with at an equivalent level of accuracy for more complex heat-release models to be worth while. For many engineering applications, Eq. (10.6) is adequate for diesel engine combustion analysis.

Additional insight can be obtained by incorporating a model for the largest of the effects omitted from Eq. (10.6), the heat transfer $dQ_{ht}/dt$ (see Chap. 12); we thereby obtain a close approximation to the *gross* heat-release rate. The integral of the gross heat-release rate over the complete combustion process should then equal (to within a few percent only, since the analysis is not exact) the mass of fuel injected $m_f$ times the fuel lower heating value $Q_{LHV}$: i.e.,

$$Q_{ch} = \int_{t_{start}}^{t_{end}} \frac{dQ_{ch}}{dt}\,dt = m_f Q_{LHV} \tag{10.7}$$

Of course, Eqs. (10.1) to (10.4), (10.6), and (10.7) also hold with crank angle $\theta$ as the independent variable instead of time $t$.

Figure 10-11 illustrates the relative magnitude of gross and net heat release, heat transfer, crevice effects, and heat of vaporization and heating up of the fuel for a turbocharged DI diesel engine operating in the mid-load, mid-speed range. The net heat release is the gross heat release due to combustion, less the heat transfer to the walls, crevice effects, and the effect of fuel vaporization and heatup (which was omitted above by neglecting the mass addition term in $dU/dt$). This last term is sufficiently small to be neglected. The enthalpy of vaporization of diesel fuel is less than 1 percent of its heating value; the energy change associated with heating up fuel vapor from injection temperature to typical compression air temperatures is about 3 percent of the fuel heating value. The heat transfer integrated over the duration of the combustion period is 10 to 25 percent of the total heat released.

**FUEL MASS BURNING RATE ANALYSIS.** If the internal energies of the fuel, air, and burned gases in Eq. (10.1) are evaluated relative to a consistent datum (such

as that described in Sec. 4.5.2), then this equation can be used to obtain an apparent *fuel mass burning rate* from cylinder pressure versus crank angle data. (With such a species energy datum the "heat release" is properly accounted for in the internal energy and enthalpy terms.) Following Krieger and Borman,[9] Eq. (10.2) can be written as

$$\frac{d}{dt}(mu) = -p\frac{dV}{dt} + \frac{dQ}{dt} + h_f\frac{dm}{dt} \tag{10.8}$$

Here $Q$ is the heat transfer to the gas within the combustion chamber (that is, $Q = -Q_{ht}$), $m$ is the mass within the combustion chamber, and $dm/dt$ has been substituted for $\dot{m}_f$.

Since the properties of the gases in the cylinder during combustion (assumed to be uniform and in chemical equilibrium at the pressure $p$ and average temperature $T$) are in general a function of $p$, $T$, and the equivalence ratio $\phi$,

$$u = u(T, p, \phi) \qquad \text{and} \qquad R = R(T, p, \phi)$$

Therefore

$$\frac{du}{dt} = \frac{\partial u}{\partial T}\frac{dT}{dt} + \frac{\partial u}{\partial p}\frac{dp}{dt} + \frac{\partial u}{\partial \phi}\frac{d\phi}{dt} \tag{10.9a}$$

$$\frac{dR}{dt} = \frac{\partial R}{\partial T}\frac{dT}{dt} + \frac{\partial R}{\partial p}\frac{dp}{dt} + \frac{\partial R}{\partial \phi}\frac{d\phi}{dt} \tag{10.9b}$$

Also,

$$\phi = \phi_0 + \left(\frac{m}{m_0} - 1\right)\frac{1 + (F/A)_0}{(F/A)_s} \tag{10.10}$$

and

$$\frac{d\phi}{dt} = \frac{1 + (F/A)_0}{(F/A)_s m_0}\frac{dm}{dt} \tag{10.11}$$

$(F/A)$ is the fuel/air ratio; the subscript 0 denotes the initial value prior to fuel injection and the subscript $s$ denotes the stoichiometric value. It then follows that

$$\frac{1}{m}\frac{dm}{dt} = \frac{-(RT/V)(dV/dt) - (\partial u/\partial p)(dp/dt) + (1/m)(dQ/dt) - CB}{u - h_f + D(\partial u/\partial \phi) - C[1 + (D/R)(\partial R/\partial \phi)]} \tag{10.12}$$

where

$$B = \frac{1}{p}\frac{dp}{dt} - \frac{1}{R}\frac{\partial R}{\partial p}\frac{dp}{dt} + \frac{1}{V}\frac{dV}{dt}$$

$$C = \frac{T(\partial u/\partial T)}{1 + (T/R)(\partial R/\partial T)}$$

$$D = \frac{[1 + (F/A)_0]m}{(F/A)_s m_0}$$



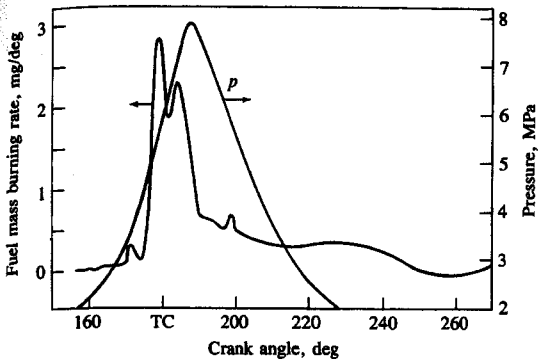


**FIGURE 10-12**
Cylinder pressure $p$ and fuel mass burning rate calculated from $p$, as a function of crank angle, using the Krieger and Borman method[9] for DI diesel engine at 3200 rev/min and full load.

Equation (10.12) can be solved numerically for $m(t)$ given $m_0$, $\phi_0$, $p(t)$, and appropriate models for the working fluid properties (see Sec. 4.7) and for the heat-transfer term $dQ/dt$ (see Chap. 12).

Figure 10-12 shows cylinder pressure data for an open chamber DI diesel and fuel mass burning rate $dm/d\theta$ calculated from that data using the above method. The heat-transfer model of Annand was used (see Sec. 12.4.3). The result obtained is an *apparent* fuel mass burning rate. It is best interpreted, after multiplying by the heating value of the fuel, as the fuel chemical-energy or heat-release rate. The *actual* fuel burning rate is unknown because not all the fuel "burns" with sufficient air available locally to produce products of *complete* combustion. About 60 percent of the fuel has burned in the first one-third of the total combustion period. The integral of the fuel mass burning rate over the combustion process should equal the total fuel mass burned; in this case it is 3 percent less than the total fuel mass injected. Note that chemical energy continues to be released well into the expansion process. The accuracy of this type of calculation then decreases, however, since errors in estimating heat transfer significantly affect the apparent fuel burning rate.

Krieger and Borman also carried out sensitivity analyses for the critical assumptions and variables. They found that the effect of dissociation of the product gases was negligible. This permits a substantial simplification of Eq. (10.12). With no dissociation, $u = u(T, \phi)$, and $R = \bar{R}/M$ can be taken as constant, since the molecular weight $M$ changes little. Then

$$\frac{dm}{dt} = \frac{[1 + (c_v/R)]p(dV/dt) + (c_v/R)V(dp/dt) - (dQ/dt)}{h_f + (c_v/R)(pV/m) - u - D(\partial u/\partial \phi)} \tag{10.13}$$

where $D$, as before, is $[1 + (F/A)_0]m/[(F/A)_s m_0]$. Given the uncertainties inherent in the heat-transfer model and the neglect of nonuniformities and crevices, Eq. (10.13) represents an adequate level of sophistication.

The other sensitivity variations studied by Krieger and Borman were: shifting of the phasing of the pressure data 2° forward and 2° backward; translating the pressure data ±34 kPa (5 lb/in$^2$); changing the heat transfer ±50 percent;

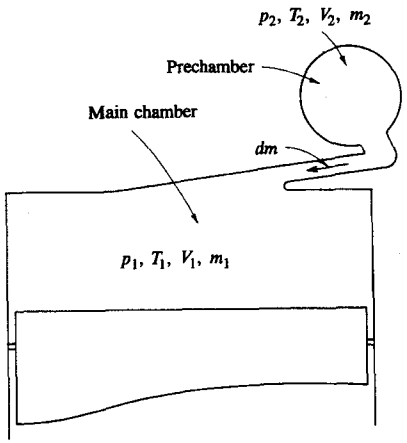


**FIGURE 10-13**
Schematic defining variables in main chamber (subscript 1) and prechamber (subscript 2) for IDI engine heat-release analysis.

increasing the initial mass 5 percent. The initial mass change had a negligible effect on the fuel burning rate calculations. The heat-transfer changes of ±50 percent changed the mass of fuel burned by about ±5 percent. The change in phasing of the pressure data was more significant. It needs to be stressed that *accurate* (in magnitude and phasing) pressure data are a most important requirement for useful heat-release or fuel mass burning rate analysis.

### 10.4.3 Indirect-Injection Engines

In IDI diesel engines, the pressures in each of the two chambers, main and auxiliary, are not the same during the combustion process. Since combustion starts in the auxiliary or prechamber, the fuel energy release in the prechamber causes the pressure there to rise above the main chamber pressure. Depending on combustion chamber design and operating conditions, the prechamber pressure rises to be 0.5 to 5 atm above that in the main chamber. This pressure difference causes a flow of fuel, air, and burning and burned gases into the main chamber, where additional energy release now occurs. The analysis of the DI diesel in the previous section was based on uniform pressure throughout the combustion chamber. For IDI engines the effect of the pressure difference between the chambers must usually be included.

Figure 10-13 shows an IDI combustion chamber divided at the nozzle into two open systems. Applying the first law [Eq. (10.1)] to the *main chamber* yields

$$\frac{dQ_1}{dt} - p_1 \frac{dV_1}{dt} + h_{2,1} \frac{dm}{dt} = \frac{dU_1}{dt} \tag{10.14}$$

and to the *auxiliary chamber* yields

$$\frac{dQ_2}{dt} - h_{2,1} \frac{dm}{dt} + h_f \frac{dm_f}{dt} = \frac{dU_2}{dt} \tag{10.15}$$



Here $dm/dt$ is the mass flow rate between the chambers with positive flow from the prechamber to the main chamber. If $dm/dt > 0$, $h_{2,1} = h_2$; if $dm/dt < 0$, $h_{2,1} = h_1$. If we define $U_1$ and $U_2$ as sensible internal energies and $h_f$ as the sensible enthalpy of the fuel, then $dQ_1/dt$ and $dQ_2/dt$ represent the net heat-release rates—the difference between the combustion energy-release rates and the rates of heat transfer to the walls.

If we use an ideal gas model for the working fluid in each chamber, with $c_v$, $c_p$, and $M$ constant, the relation $p_1 V_1 = m_1 R T_1$ and $p_2 V_2 = m_2 R T_2$ can be used to eliminate $m$ and $T$ from the $dU/dt$ terms and, with the fact that $h_{s,f} = 0$, can be used to write Eqs. (10.14) and (10.15) as

$$\frac{dQ_1}{dt} = \frac{\gamma}{\gamma - 1} p_1 \frac{dV_1}{dt} + \frac{1}{\gamma - 1} V_1 \frac{dp_1}{dt} - c_p T_{2,1} \frac{dm}{dt} \tag{10.16}$$

$$\frac{dQ_2}{dt} = \frac{1}{\gamma - 1} V_2 \frac{dp_2}{dt} + c_p T_{2,1} \frac{dm}{dt} \tag{10.17}$$

When Eqs. (10.16) and (10.17) are added together, the term representing the enthalpy flux between the two chambers cancels out, and the following equation for *total* net heat-release results:

$$\frac{dQ}{dt} = \frac{dQ_1}{dt} + \frac{dQ_2}{dt} = \frac{\gamma}{\gamma - 1} p_1 \frac{dV_1}{dt} + \frac{1}{\gamma - 1} \left( V_1 \frac{dp_1}{dt} + V_2 \frac{dp_2}{dt} \right) \tag{10.18}$$

The comments made in the previous section regarding the interpretation of the net heat release (it is the gross heat release due to combustion less the heat transfer to the walls, and other smaller energy transfers due to crevices, fuel vaporization, and heatup) also hold here.

In practice, Eq. (10.18) is difficult to use since it requires experimental data for both the main and auxiliary chamber pressures throughout the combustion process. Access for two pressure transducers through the cylinder head is not often available; even when access can be achieved, the task of obtaining pressure data from two different transducers under the demanding thermal loading conditions found in IDI diesels, of sufficient accuracy such that the difference between the pressures (of order 0.5 to 5 atm) at pressure levels of 60 to 80 atm can be interpreted, requires extreme diligence in technique.[10,11] Figure 10-14*a* and *b* shows apparent net heat-release rate profiles for an IDI diesel obtained using Eq. (10.18) with $\gamma = 1.35$.[11] Curves of $dQ/dt$ and $dQ/d\theta$ are shown at three different speeds and essentially constant fuel mass injected per cycle. While the absolute heat-release rates increase with increasing speed, the relative rates are essentially independent of speed, indicating that combustion rates, which depend on fuel-air mixing rates, scale approximately with engine speed.

Equation (10.18) (or its equivalent) has been used assuming $p_2 = p_1$ and using either main chamber or auxiliary chamber pressure data alone. The error associated with this approximation can be estimated as follows. If we write $p_2 =$

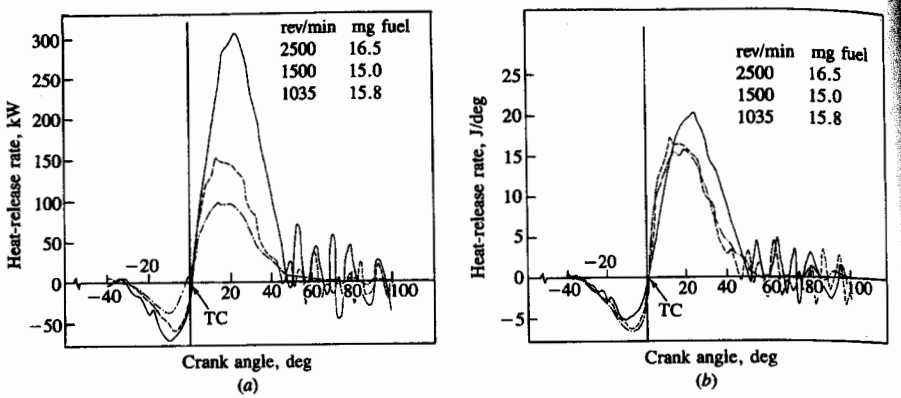


**FIGURE 10-14**
Calculated net heat-release-rate profiles for IDI diesel engine at constant load ($0.29 \leq \phi \leq 0.32$). (*a*) Heat-release rate in kilowatts. (*b*) Heat-release rate in joules per degree.[11]

$p_1 + \Delta p$ then Eq. (10.18) becomes

$$\frac{dQ}{dt} = \frac{\gamma}{\gamma - 1} p_1 \frac{dV_1}{dt} + \frac{V_1 + V_2}{\gamma - 1} \frac{dp_1}{dt} + \frac{V_2}{\gamma - 1} \frac{d(\Delta p)}{dt} \tag{10.19}$$

If the last term is omitted, Eq. (10.19) is identical to Eq. (10.6) derived for the DI diesel. Since the term $V(dp_1/dt)/(\gamma - 1)$ is much larger than the first term on the right-hand side of Eq. (10.19) during the early stages of the combustion process, the error involved in omitting the last term is given to a good approximation by $[V_2/(V_1 + V_2)]d(\Delta p)/dp_1$. In the initial stages of combustion this error can be quite large (of order 0.25 based on data in Ref. 10 close to TC). Later in the combustion process it becomes negligible (of order a few percent after 20° ATC).[10] Thus, neglecting $\Delta p$ will lead to errors in predicting the initial heat-release *rate*. The magnitude of the error will depend on the design of the combustion chamber and on engine speed and load (with more restricted passageways, higher loads and speeds, giving higher values of $\Delta p$ and, therefore, greater error). Later in the combustion process the error is much less, so *integrated* heat-release data derived ignoring $\Delta p$ will show a smaller error.

A model analogous to the above, but using the approach of Krieger and Borman[9] (see Sec. 10.4.2), for the IDI diesel has been developed and used by Watson and Kamel.[10] The energy conservation equation for an *open* system developed in Sec. 14.2.2, with energy and enthalpy modeled using a consistent datum (see Sec. 4.5.2), with appropriate models for convective and radiation heat transfer and for gas properties, was applied to the main chamber and also to the prechamber. These equations were solved using accurately measured main chamber and prechamber pressure data to determine the apparent rate of heat release (here, the rate of fuel burning multiplied by the fuel heating value) in the main chamber and prechambers through the combustion process. The engine was a Ricardo Comet swirl chamber IDI design. Some results are shown in Fig.



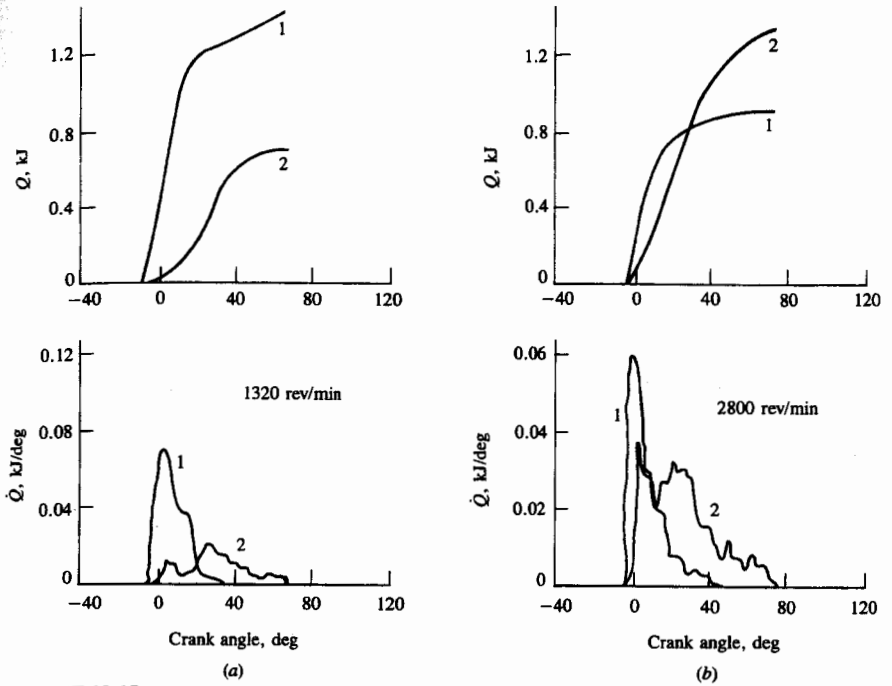


**FIGURE 10-15**
Calculated gross heat-release rates in IDI swirl-chamber diesel engine at full load. 1 Prechamber heat release. 2 Main chamber heat release. Top figures: integrated heat release. Bottom figures: heat-release rate. (*a*) 1320 rev/min; (*b*) 2800 rev/min.[10]

10-15. For this particular engine, at low engine speeds two-thirds of the heat release occurs in the prechamber; at higher engine speeds about two-thirds of the heat release occurs in the main chamber.

## 10.5 FUEL SPRAY BEHAVIOR

### 10.5.1 Fuel Injection

The fuel is introduced into the cylinder of a diesel engine through a nozzle with a large pressure differential across the nozzle orifice. The cylinder pressure at injection is typically in the range 50 to 100 atm. Fuel injection pressures in the range 200 to 1700 atm are used depending on the engine size and type of combustion system employed. These large pressure differences across the injector nozzle are required so that the injected liquid fuel jet will enter the chamber at sufficiently high velocity to (1) atomize into small-sized droplets to enable rapid evaporation and (2) traverse the combustion chamber in the time available and fully utilize the air charge.

Examples of common diesel fuel-injection systems were described briefly in Sec. 1.7 and illustrated in Figs. 1-17 to 1-19. (See also Refs. 12 and 13 for more

extensive descriptions of diesel fuel-injection systems.) The task of the fuel-injection system is to meter the appropriate quantity of fuel for the given engine speed and load to each cylinder, each cycle, and inject that fuel at the appropriate time in the cycle at the desired rate with the spray configuration required for the particular combustion chamber employed. It is important that injection begin and end cleanly, and avoid any secondary injections.

To accomplish this task, fuel is usually drawn from the fuel tank by a supply pump, and forced through a filter to the injection pump. The injection pump sends fuel under pressure to the nozzle pipes which carry fuel to the injector nozzles located in each cylinder head. Excess fuel goes back to the fuel tank. Figures 1-17 and 1-19 show two common versions of fuel systems used with multicylinder engines in the 20 to 100 kW per cylinder brake power range which operate with injection pressures between about 300 and 1200 atm.

In-line injection pumps (Fig. 1-17) are used in engines in the 40 to 100 kW per cylinder maximum power range. They contain a plunger and barrel assembly for each engine cylinder. Each plunger is raised by a cam on the pump camshaft and is forced back by the plunger return spring. The plunger stroke is fixed. The plunger fits sufficiently accurately within the barrel to seal without additional sealing elements, even at high pressures and low speeds. The amount of fuel delivered is altered by varying the *effective* plunger stroke. This is achieved by means of a control rod or rack, which moves in the pump housing and rotates the plunger via a ring gear or linkage lever on the control sleeve. The plunger chamber above the plunger is always connected with the chamber below the plunger helix by a vertical groove or bore in the plunger. Delivery ceases when the plunger helix exposes the intake port (port opening), thus connecting the plunger chamber with the suction gallery. When this takes place depends on the rotational position of the plunger. In the case of a lower helix, delivery always starts (port closing) at the same time, but ends sooner or later depending on the rotational position of the plunger. With a plunger with an upper helix, port closing (start of delivery) not port opening is controlled by the helix and is varied by rotating the plunger. Figure 1-18 illustrates how the plunger helix controls fuel delivery.[14]

Distributor-type fuel-injection pumps (such as that illustrated in Fig. 1-19) are normally used in multicylinder engines with less than 30 kW per cylinder maximum power with injection pressures up to 750 atm. These pumps have only one plunger and barrel. The pump plunger is made to describe a combined rotary and stroke movement by the rotating cam plate. The fuel is accurately metered to each injection nozzle in turn by this plunger which simultaneously acts as the distributor. Such units are more compact and cheaper than in-line pumps but cannot achieve such high injection pressures. The distributor-type fuel-injection pump is combined with the automatic timing device, governor, and supply pump to form a single unit.

Single-barrel injection pumps are used on small one- and two-cylinder diesel engines, as well as large engines with outputs of more than 100 kW per cylinder. Figure 10-16 shows the layout of the injection system and a section



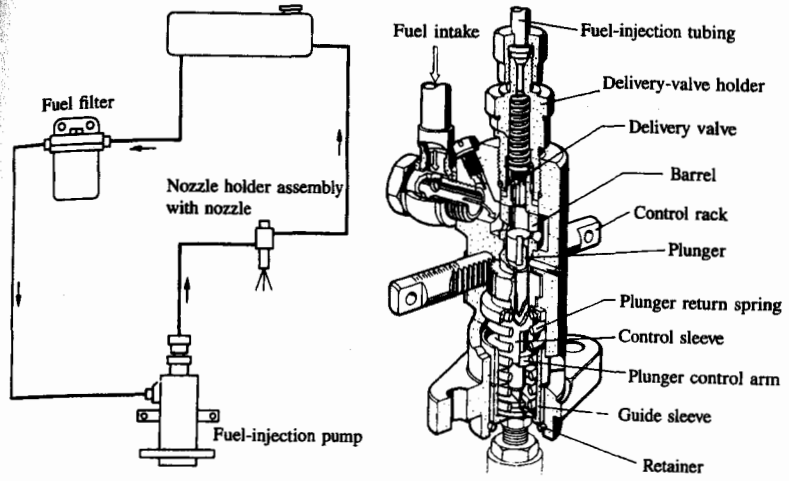


**FIGURE 10-16**
Fuel-injection system with single-barrel pump. Left: system layout. Right: section through fuel-injection pump. (*Courtesy Robert Bosch GmbH and SAE.*[14])

through the fuel-injection pump.[14] Such pumps are driven by an auxiliary cam on the engine camshaft. Also used extensively on larger engines are unit injectors where the pump and injector nozzle are combined into a single unit. An example of a unit injector and its driving mechanism used on a large two-stroke cycle diesel engine is shown in Fig. 10-17. Fuel, supplied to the injector through a fuel-distributing manifold, enters the cavity or plunger chamber ahead of the plunger through a metering orifice. When fuel is to be injected, the cam via the rocker arm pushes down the plunger, closing the metering orifice and compressing the fuel, causing it to flow through check valves and discharge into the cylinder through the injector nozzles or orifices. The amount of fuel injected is controlled by the rack, which controls the spill of fuel into the fuel drain manifold by rotating the plunger with its helical relief section via the gear.

The most important part of the injection system is the nozzle. Examples of different nozzle types and a nozzle holder assembly are shown in Fig. 1-18. The nozzles shown are fluid-controlled needle valves where the needle is forced against the valve seat by a spring. The pressure of the fuel in the pressure chamber above the nozzle aperture opens the nozzle by the axial force it exerts on the conical surface of the nozzle needle. Needle valves are used to prevent dribble from the nozzles when injection is not occurring. It is important to keep the volume of fuel left between the needle and nozzle orifices (the sac volume) as small as possible to prevent any fuel flowing into the cylinder after injection is over, to control hydrocarbon emissions (see Sec. 11.4.4). Multihole nozzles are used with most direct-injection systems; the M.A.N. "M" system uses a single-hole nozzle. Pintle nozzles, where the needle projects into and through the nozzle hole, are used in indirect-injection engine systems. The shape of the pin on the

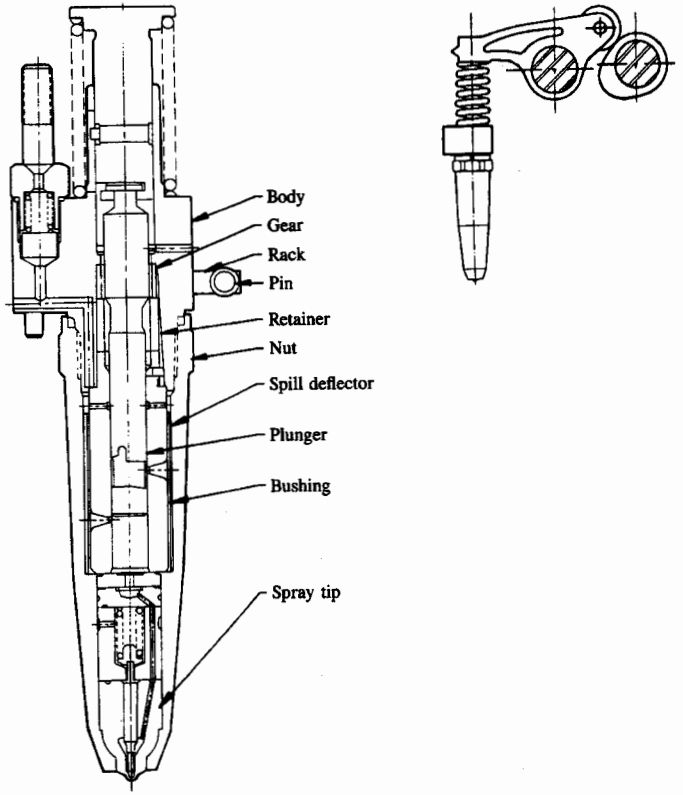


**FIGURE 10-17**
Unit fuel injector and its driving mechanism, typically used in large diesel engines.[15]

end of the nozzle needle controls the spray pattern and fuel-delivery characteristics. Auxiliary nozzle holes are sometimes used to produce an auxiliary smaller spray to aid ignition and starting. Open nozzle orifices, without a needle, are also used.

The technology for electronic control of injection is now available. In an electronic injector, such as that shown in Fig. 10-18, a solenoid operated control valve performs the injection timing and metering functions in a fashion analogous to the ports and helices of the mechanical injector. Solenoid valve closure initiates pressurization and injection, and opening causes injection pressure decay and end of injection. Duration of valve closure determines the quantity of fuel injected. The unit shown uses camshaft/rocker arm driven plungers to generate the injection pressure, and employs needle-valve nozzles of conventional design. Increased flexibility in fuel metering and timing and simpler injector mechanical design are important advantages.[16]

Accurate predictions of fuel behavior within the injection system require



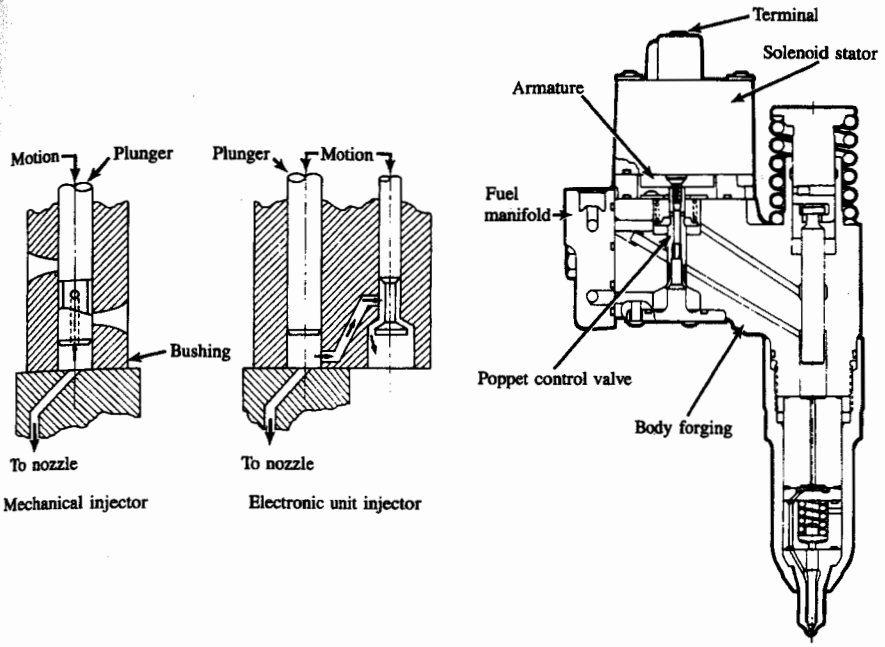


**FIGURE 10-18**
Electronically controlled unit fuel-injection system.[16]

sophisticated hydraulic models: Hiroyasu[17] provides an extensive reference list of such models. However, approximate estimates of the injection rate through the injector nozzles can be made as follows. If the pressure upstream of the injector nozzle(s) can be estimated or measured, and assuming the flow through each nozzle is quasi steady, incompressible, and one dimensional, the mass flow rate of fuel injected through the nozzle $\dot{m}_f$ is given by

$$\dot{m}_f = C_D A_n \sqrt{2\rho_f \Delta p} \tag{10.20}$$

where $A_n$ is the nozzle minimum area, $C_D$ the discharge coefficient, $\rho_f$ the fuel density, and $\Delta p$ the pressure drop across the nozzle. If the pressure drop across the nozzle and the nozzle open area are essentially constant during the injection period, the mass of fuel injected is then

$$m_f = C_D A_n \sqrt{2\rho_f \Delta p}\, \frac{\Delta\theta}{360N} \tag{10.21}$$

where $\Delta\theta$ is the nozzle open period in crank angle degrees and $N$ is engine speed. Equations (10.20) and (10.21) illustrate the dependence of injected amounts of fuel on injection system and engine parameters.

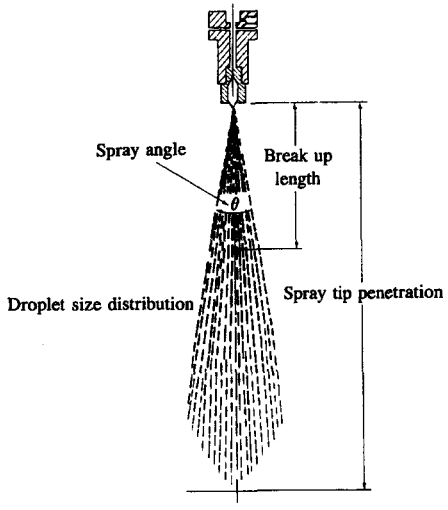


**FIGURE 10-19**
Schematic of diesel fuel spray defining its major parameters.[18]

### 10.5.2 Overall Spray Structure

The fuel is introduced into the combustion chamber of a diesel engine through one or more nozzles or orifices with a large pressure differential between the fuel supply line and the cylinder. Different designs of nozzle are used (e.g., single-orifice, multiorifice, throttle, or pintle; see Fig. 1-18), depending on the needs of the combustion system employed. Standard diesel injectors usually operate with fuel-injection pressures between 200 and 1700 atm. At time of injection, the air in the cylinder has a pressure of 50 to 100 atm, temperature about 1000 K, and density between 15 and 25 kg/m$^3$. Nozzle diameters cover the range 0.2 to 1 mm diameter, with length/diameter ratios from 2 to 8. Typical distillate diesel fuel properties are: relative specific gravity of 0.8, viscosity between 3 and 10 kg/m·s and surface tension about $3 \times 10^{-2}$ N/m (at 300 K). Figure 10-19 illustrates the structure of a typical DI engine fuel spray. As the liquid jet leaves the nozzle it becomes turbulent and spreads out as it entrains and mixes with the surrounding air. The initial jet velocity is greater than $10^2$ m/s. The outer surface of the jet breaks up into drops of order 10 $\mu$m diameter, close to the nozzle exit. The liquid column leaving the nozzle disintegrates within the cylinder over a finite length called the *breakup length* into drops of different sizes. As one moves away from the nozzle, the mass of air within the spray increases, the spray diverges, its width increases, and the velocity decreases. The fuel drops evaporate as this air-entrainment process proceeds. The tip of the spray penetrates further into the combustion chamber as injection proceeds, but at a decreasing rate. Figure 10-20 shows photographs of a diesel fuel spray injected into quiescent air in a rapid-compression machine which simulates diesel conditions.[19] Two different photographic techniques, back lighting and shadowgraph,† have been used to distinguish the liquid-containing core of the jet and the extent of the fuel vapor region of the spray which surrounds the liquid core. The region of the jet closest to the nozzle (until injection ceases at 3.3 ms) contains liquid drops and ligaments; the major region of the spray is a substantial vapor cloud around this narrow core which contains liquid fuel.



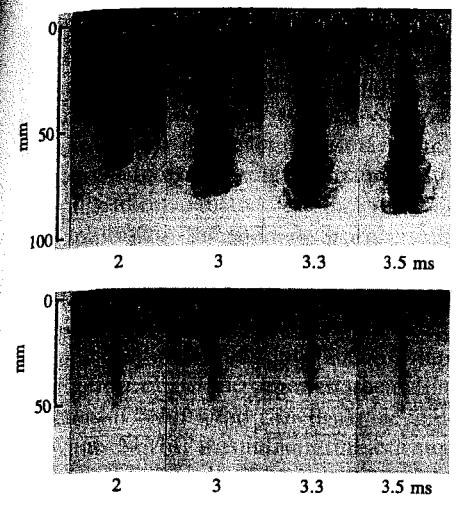


**FIGURE 10-20**
Shadowgraph and back-illuminated photographs of evaporating spray injected into nitrogen at 3.4 MPa and 670 K in rapid-compression machine. Times in milliseconds are after start of injection: injection duration 3.3 ms. Top (shadowgraph) photographs show full vapor and liquid region. Bottom (back-illuminated) photographs only show liquid-containing core.[19]

Different spray configurations are used in the different diesel combustion systems described earlier in this chapter. The simplest configuration involves multiple sprays injected into quiescent air in the largest-size diesels (Fig. 10-1*a*). Figures 10-19 and 10-20 illustrate the essential features of each spray under these circumstances until interactions with the wall occur. Each liquid fuel jet atomizes into drops and ligaments at the exit from the nozzle orifice (or shortly thereafter). The spray entrains air, spreads out, and slows down as the mass flow in the spray increases. The droplets on the outer edge of the spray evaporate first, creating a fuel vapor–air mixture sheath around the liquid-containing core. The highest velocities are on the jet axis. The equivalence ratio is highest on the centerline (and fuel-rich along most of the jet), decreasing to zero (unmixed air) at the spray boundary. Once the sprays have penetrated to the outer regions of the combustion chamber, they interact with the chamber walls. The spray is then forced to flow tangentially along the wall. Eventually the sprays from multihole nozzles

† The back lighting identifies regions where sufficient liquid fuel (as ligaments or drops) is present to attenuate the light. The shadowgraph technique responds to density gradients in the test section, so it identifies regions where fuel vapor exists.

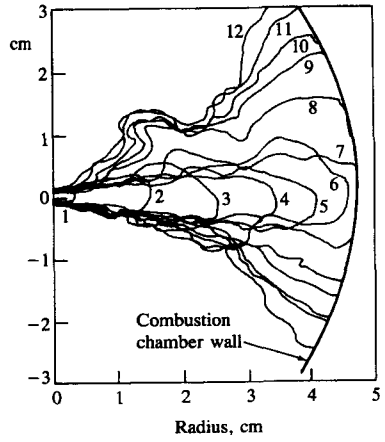


**FIGURE 10-21**
Sketches of outer vapor boundary of diesel fuel spray from 12 successive frames of rapid-compression-machine high-speed shadowgraph movie showing interaction of vaporizing spray with cylindrical wall of combustion chamber. Injection pressure 60 MPa. Time between frames 0.14 ms.[20]

interact with one another. Figure 10-21 shows diesel fuel sprays interacting with the cylindrical outer wall of a disc-shaped combustion chamber in a rapid-compression machine, under typical diesel-injection conditions. The cylinder wall causes the spray to split with about half flowing circumferentially in either direction. Adjacent sprays then interact forcing the flow radially inward toward the chamber axis.[20]

Most of the other combustion systems in Figs. 10-1 and 10-2 use air swirl to increase fuel-air mixing rates. A schematic of the spray pattern which results when a fuel jet is injected radially outward into a swirling flow is shown in Fig. 10-22. Because there is now relative motion in both radial and tangential directions between the initial jet and the air, the structure of the jet is more complex. As the spray entrains air and slows down it becomes increasingly bent toward the swirl direction; for the same injection conditions it will penetrate less with swirl than without swirl. An important feature of the spray is the large vapor-containing region downstream of the liquid-containing core. Figure 10-23 shows schlieren photographs of four fuel jets injected on the axis of an IDI diesel engine

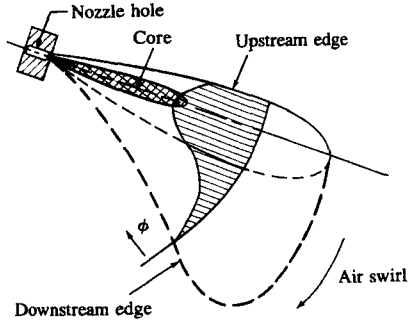


**FIGURE 10-22**
Schematic of fuel spray injected radially outward from the chamber axis into swirling air flow. Shape of equivalence ratio ($\phi$) distribution within jet is indicated.



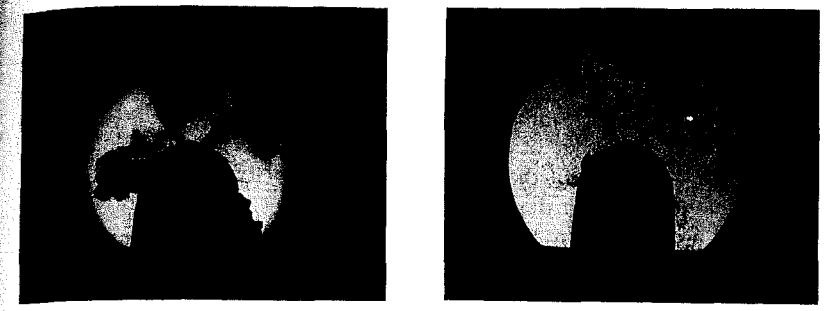

**FIGURE 10-23**
Schlieren photographs of vaporizing sprays injected into swirling air flow in transparent prechamber of special IDI diesel.[21] Left: high sensitivity, showing boundaries of the vapor regions of spray. Right: low sensitivity, showing liquid-containing core (dark) in relation to vapor regions (mottled).

prechamber with high clockwise swirl. The photograph on the left, with high sensitivity, shows the outer boundary of the fuel vapor region of the spray; the low-sensitivity photograph on the right locates the liquid phase regions of the spray.[21] The interaction between the swirl and both liquid and vapor spray regions is evident, as is the spray interaction with the chamber wall.

Other spray flow patterns are used. The spray may enter the swirling air flow tangentially as in the M.A.N. "M" system shown in Fig. 10-1*c*. The spray then interacts immediately with the combustion chamber walls.

To couple the spray-development process with the ignition phase of the combustion, it is important to know which regions of the spray contain the fuel injected at the beginning of the injection process. These regions of the sprays are likely to autoignite first. Each spray develops as follows. At the start of injection the liquid fuel enters the quiescent air charge, atomizes, moves outward from the nozzle, and slows down rapidly as air is entrained into the spray and accelerated. This start-up process forms a vortex or "puff" at the head of the spray. The injected fuel which follows encounters less resistance; thus drops from that fuel overtake the drops from first-injected fuel, forcing them outward toward the periphery of the spray. At the tip of the unsteady spray the drops meet the highest aerodynamic resistance and slow down, but the spray continues to penetrate the air charge because droplets retarded at the tip are continually replaced by new higher-momentum later-injected drops.[22] Accordingly, droplets in the periphery of the spray and behind the tip of the spray come from the earliest injected fuel.[23] As Figs. 10-20 and 10-23 indicate, these drops evaporate quickly.

### 10.5.3 Atomization

Under diesel engine injection conditions, the fuel jet usually forms a cone-shaped spray at the nozzle exit. This type of behavior is classified as the atomization breakup regime, and it produces droplets with sizes very much less than the nozzle exit diameter. This behavior is different from other modes of liquid jet

breakup. At low jet velocity, in the Rayleigh regime, breakup is due to the unstable growth of surface waves caused by surface tension and results in drops larger than the jet diameter. As jet velocity is increased, forces due to the relative motion of the jet and the surrounding air augment the surface tension force, and lead to drop sizes of the order of the jet diameter. This is called the first wind-induced breakup regime. A further increase in jet velocity results in breakup characterized by divergence of the jet spray after an intact or undisturbed length downstream of the nozzle. In this second wind-induced breakup regime, the unstable growth of short-wavelength waves induced by the relative motion between the liquid and surrounding air produces droplets whose average size is much less than the jet diameter. Further increases in jet velocity lead to breakup in the atomization regime, where the breakup of the outer surface of the jet occurs at, or before, the nozzle exit plane and results in droplets whose average diameter is much smaller than the nozzle diameter. Aerodynamic interactions at the liquid/gas interface appear to be one major component of the atomization mechanism in this regime.[22, 24]

A sequence of very short time exposure photographs of the emergence of a liquid jet from a nozzle of 0.34 mm diameter and $L_n/d_n = 4$ into high-pressure nitrogen at ambient temperature is shown in Fig. 10-24. The figure shows how the spray tip penetrates and the spray spreads during the early part of its travel.[25] Data such as these were used to examine the dependence of the spray development on gas and liquid density, liquid viscosity, and nozzle geometry.[24–26] The effects of the most significant variables, gas/liquid density ratio and nozzle geometry, on initial jet spreading angle are shown in Fig. 10-25. For a given geometry (cylindrical hole and length/diameter = 4), the initial jet spreading or spray angle increases with increasing gas/liquid density ratio as shown in Fig. 10-25*a*. Typical density ratios for diesel injection conditions are between $15 \times 10^{-3}$ and $30 \times 10^{-3}$. Of several different nozzle geometry parameters examined, the length/diameter ratio proved to be the most significant (see Fig. 10-25*b*).

For jets in the atomization regime, the spray angle $\theta$ was found to follow the relationship

$$\tan \frac{\theta}{2} = \frac{1}{A} 4\pi \left(\frac{\rho_g}{\rho_l}\right)^{1/2} \frac{\sqrt{3}}{6} \tag{10.22}$$

where $\rho_g$ and $\rho_l$ are gas and liquid densities and $A$ is a constant for a given nozzle geometry.† The data in Fig. 10-25*a* are fitted by $A = 4.9$. This behavior is in accord with the theory that aerodynamic interactions are largely responsible for jet breakup. Note that the data in Fig. 10-25*b* show a continuous trend as the jet breakup regime makes a transition from second wind-induced breakup (solid

† An empirical equation for $A$ is $A = 3.0 + 0.28\,(L_n/d_n)$, where $L_n/d_n$ is the length/diameter ratio of the nozzle.[25]



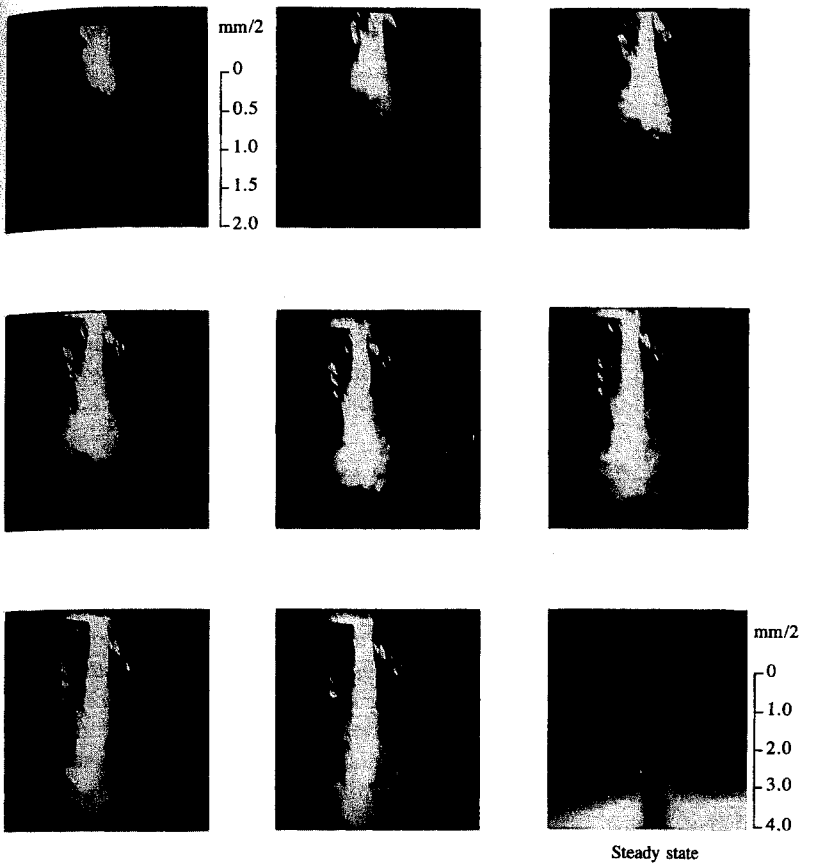


**FIGURE 10-24**
Photographs showing initial emergence and steady state (bottom right) of high-pressure liquid spray. Time between frames 2.1 $\mu$s. Liquid: water. Gas: nitrogen at 1380 kPa. $\Delta p$ across nozzle 11 MPa. Nozzle diameter 0.34 mm.[25]

symbols) to atomization regime breakup (open symbols). The growth of aerodynamic surface waves is known to be responsible for jet breakup in the second wind-induced breakup regime. Such a mechanism can explain the observed data trends in the atomization regime, if an additional mechanism is invoked to explain nozzle geometry effects. One possible additional mechanism is liquid cavitation. A criterion for the onset of jet atomization at the nozzle exit plane was developed. For $(\rho_l/\rho_g)(\mathrm{Re}_l/\mathrm{We}_l)^2 > 1$ (which is true for distillate fuel injection applications) the design criterion is

$$\left(\frac{\rho_l}{\rho_g}\right)^{1/2} < k \tag{10.23}$$

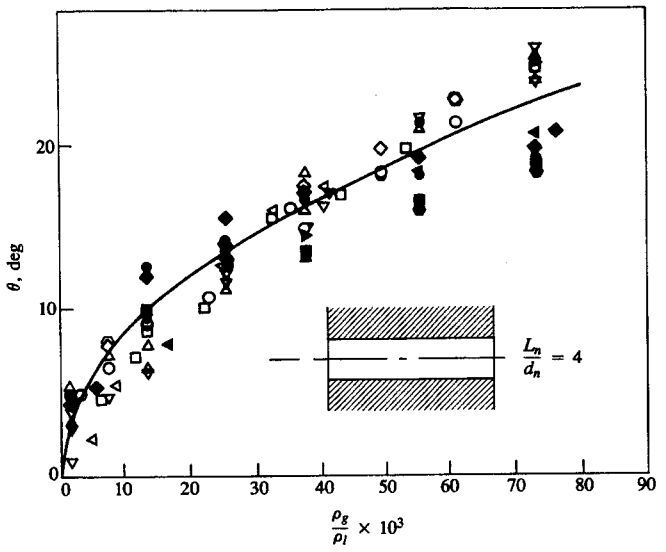


(a)

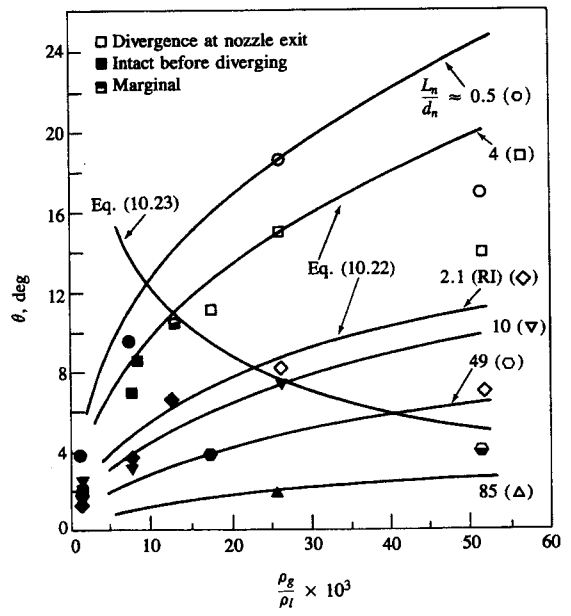


(b)

**FIGURE 10-25**
(*a*) Initial spray angle of atomizing jets versus density ratio ($\rho_g/\rho_l$ = gas density/liquid density) for fixed nozzle geometry shown. Various fluids and gases at liquid pressures of 3.4–92 MPa. Nozzle diameters $d_n$ = 0.254, 0.343, and 0.61 mm.[22] (*b*) Initial spray angle versus density ratio for a wide range of nozzle geometries. $L_n/d_n$ = nozzle length/diameter ratio (RI = rounded inlet geometry). Solid symbols indicate jets which break up and diverge downstream of nozzle exit. Open symbols indicate jet breakup at nozzle exit.[25]



where $k$ is an empirical constant depending on nozzle geometry in the range 6 to 12 ($k = 18.3/\sqrt{A}$).

Jet breakup trends can be summarized as follows. The initial jet divergence angles increase with increasing gas density. Divergence begins progressively closer to the nozzle as gas density increases until it reaches the nozzle exit. Jet divergence angles increase with decreasing fuel viscosity; divergence begins at the nozzle exit once the liquid viscosity is below a certain level. Nozzle design affects the onset of the jet atomization regime. Jet divergence angles decrease with increasing nozzle length. For the same length, rounded inlet nozzles produce less divergent jets than sharp-edged inlet nozzles. The initial jet divergence angle and intact spray length are quasi steady with respect to changes in operating conditions which occur on time scales longer than about 20 $\mu$s.[25] Note that while all these results were obtained under conditions where evaporation was not occurring, the initial spray-development processes are not significantly affected by evaporation (see Sec. 10.5.6).

### 10.5.4 Spray Penetration

The speed and extent to which the fuel spray penetrates across the combustion chamber has an important influence on air utilization and fuel-air mixing rates. In some engine designs, where the walls are hot and high air swirl is present, fuel impingement on the walls is desired. However, in multispray DI diesel combustion systems, overpenetration gives impingement of liquid fuel on cool surfaces which, especially with little or no air swirl, lowers mixing rates and increases emissions of unburned and partially burned species. Yet underpenetration results in poor air utilization since the air on the periphery of the chamber does not then contact the fuel. Thus, the penetration of liquid fuel sprays under conditions typical of those found in diesel engines has been extensively studied.

Many correlations based on experimental data and turbulent gas jet theory have been proposed for fuel spray penetration.[17] These predict the penetration $S$ of the fuel spray tip across the combustion chamber for injection into quiescent air, as occurs in larger DI engines, as a function of time. An evaluation of these correlations[27] indicated that the formula developed by Dent,[28] based on a gas jet mixing model for the spray, best predicts the data:†

$$S = 3.07\left(\frac{\Delta p}{\rho_g}\right)^{1/4}(td_n)^{1/2}\left(\frac{294}{T_g}\right)^{1/4} \tag{10.24}$$

where $\Delta p$ is the pressure drop across the nozzle, $t$ is time after the start of injection, and $d_n$ is the nozzle diameter. All quantities are expressed in SI units: $t$ in

† For nozzles where $2 \le L_n/d_n \le 4$, and for $t > 0.5$ ms. At exceptionally high chamber densities ($p > 100$ atm) Eq. (10.24) overpredicts penetration.

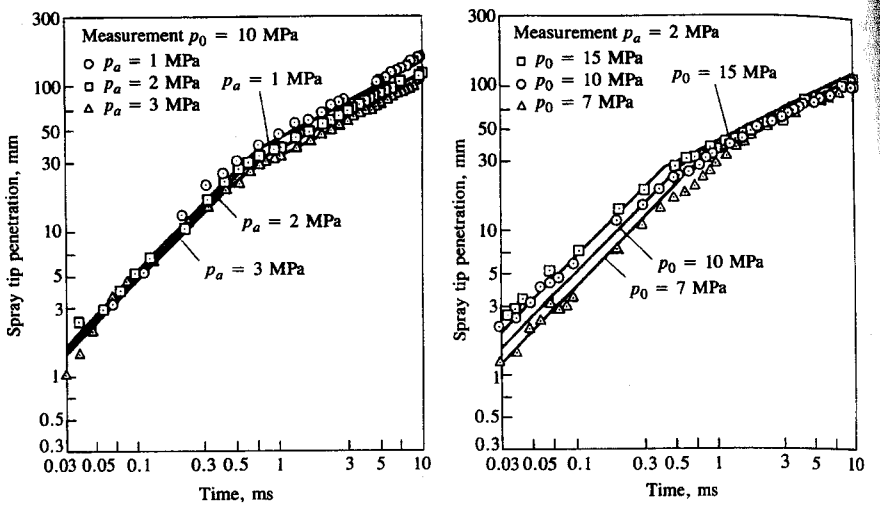


**FIGURE 10-26**
Spray tip penetration as function of time at various ambient pressures ($p_a$) and injection pressures ($p_0$). Fuel jets injected into quiescent air at room temperature.[29]

seconds, $S$ and $d_n$ in meters, $\Delta p$ in pascals, $\rho_g$ in kilograms per cubic meter, and $T_g$ in kelvins.

More detailed studies have examined the spray tip location as a function of time, following start of a diesel injection process in high-pressure bombs. Data taken by Hiroyasu *et al.*,[29] shown in Fig. 10-26, illustrate the sensitivity of the spray tip position as a function of time to ambient gas state and injection pressure for fuel jets injected into quiescent air at room temperature. These data show that the initial spray tip penetration increases linearly with time $t$ (i.e., the spray tip velocity is constant) and, following jet breakup, then increase as $\sqrt{t}$. Injection pressure has a more significant effect on the initial motion before breakup; ambient gas density has its major impact on the motion after breakup. Hiroyasu *et al.* correlated their data for spray tip penetration $S$(m) versus time as

$$t < t_{\text{break}}: \quad S = 0.39\left(\frac{2\Delta p}{\rho_l}\right)^{1/2} t$$

$$t > t_{\text{break}}: \quad S = 2.95\left(\frac{\Delta p}{\rho_g}\right)^{1/4} (d_n t)^{1/2} \tag{10.25}$$

where

$$t_{\text{break}} = \frac{29\rho_l d_n}{(\rho_g \Delta p)^{1/2}} \tag{10.26}$$

and $\Delta p$ is the pressure drop across the nozzle (pascals), $\rho_l$ and $\rho_g$ are the liquid and gas densities, respectively (in kilograms per cubic meter), $d_n$ is the nozzle



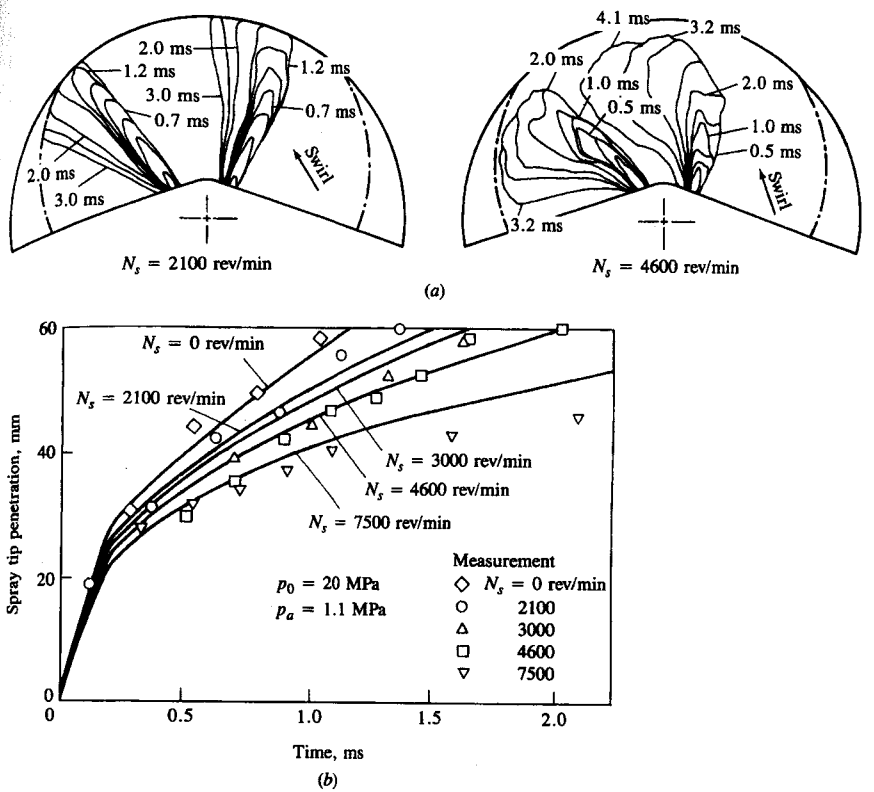


**FIGURE 10-27**
(*a*) Measured outer boundary of sprays injected into swirling air flow. (*b*) Spray tip penetration as a function of time for different swirl rates. Solid lines show Eq. (10.27).[29]

diameter (meters), and $t$ is time (seconds). The results of Reitz and Bracco[25] indicate that the breakup or intact length depends on nozzle geometry details in addition to the diameter (see Fig. 10-25*b*). Note that under high injection pressures and nozzle geometries with short length/diameter ratios, the intact or breakup length becomes very short; breakup can occur at the nozzle exit plane.

The effect of combustion air swirl on spray penetration is shown in Fig. 10-27. Figure 10-27*a* shows how the spray shape and location changes as swirl is increased; Fig. 10-27*b* shows how spray tip penetration varies with time and swirl rate.[29] These authors related their data on spray tip penetration with swirl, $S_s$, through a correlation factor to the equivalent penetration, $S$, without swirl given by Eq. (10.25):

$$\frac{S_s}{S} = \left(1 + \frac{\pi R_s N S}{30 v_j}\right)^{-1} \tag{10.27}$$

where $R_s$ is the swirl ratio which equals the swirl rate in revolutions per minute divided by the engine speed $N$ (revolutions per minute), and $v_j$ is the initial fuel jet velocity (meters per second). The curves in Fig. 10-27*b* correspond to Eq. (10.27). Swirl both reduces the penetration of the spray and spreads out the spray more rapidly.

### 10.5.5 Droplet Size Distribution

Previous sections in Sec. 10.5 have discussed the overall characteristics of the diesel engine fuel spray—its spreading rate and penetration into the combustion chamber. While the distribution of fuel via the spray trajectory throughout the combustion chamber is important, atomization of the liquid fuel into a large number of small drops is also necessary to create a large surface area across which liquid fuel can evaporate. Here we review how the drop size distribution in the fuel spray depends on injection parameters and the air and fuel properties. Since the measurement of droplet characteristics in an operating diesel engine is extremely difficult, most results have come from studies of fuel injection into constant-volume chambers filled with high-pressure quiescent air at room temperature.

During the injection period, the injection conditions such as injection pressure, nozzle orifice area, and injection rate may vary. Consequently, the droplet size distribution at a given location in the spray may also change with time during the injection period. In addition, since the details of the atomization process are different in the spray core and at the spray edge, and the trajectories of individual drops depend on their size, initial velocity, and location within the spray, the drop size distribution will vary with position within the spray.[29] None of these variations has yet been adequately quantified.

The aerodynamic theory of jet breakup in the atomization regime summarized in Sec. 10.5.3 (which is based on work by G. I. Taylor) leads to the prediction that the initial average drop diameter $D_d$ is proportional to the length of the most unstable surface waves:[22]

$$\bar{D}_d = C \frac{2\pi\sigma}{\rho_g v_r^2} \lambda^* \tag{10.28}$$

where $\sigma$ is the liquid-fuel surface tension, $\rho_g$ is the gas density, $v_r$ is the relative velocity between the liquid and gas (taken as the mean injection velocity $v_j$), $C$ is a constant of order unity, and $\lambda^*$ is the dimensionless wavelength of the fastest growing wave. $\lambda^*$ is a function of the dimensionless number $(\rho_l/\rho_g)(\mathrm{Re}_j/\mathrm{We}_j)^2$, where the jet Reynolds and Weber numbers are given by $\mathrm{Re}_j = \rho_l v_j d_n/\mu_l$ and $\mathrm{We}_j = \rho_l v_j^2 d_n/\sigma$ and $d_n$ is the nozzle orifice diameter. $\lambda^*$ goes to 3/2 as this number increases above unity. Near the edge of the spray close to the nozzle, this equation predicts observed drop size trends with respect to injection velocity, fuel properties, nozzle $L/d$, and nozzle diameter, though measured mean drop sizes are larger by factors of 2 to 3.[30] However, within the dense early region of the spray, secondary atomization phenomena—coalescence and breakup—occur



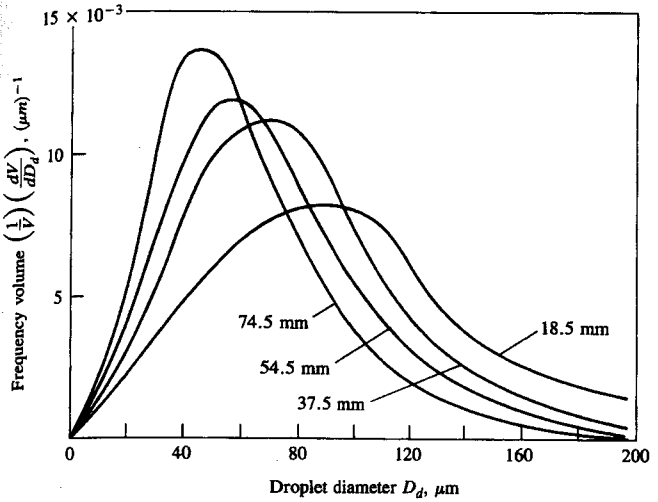


**FIGURE 10-28**
Droplet size distribution in diesel fuel spray injected through throttling pintle nozzle into quiescent room-temperature air at 11 atm. Nozzle opening pressure 9.9 MPa. Pump speed 500 rev/min. Droplets are sampled well downstream of injector at given radial distances from spray axis.[32]

which will change the droplet size distribution and mean diameter. The downstream drop size in the solid-cone sprays used in diesel-injection systems is markedly influenced by both drop coalescence and breakup. Eventually a balance is reached as coalescence decreases (due to the expansion of the spray) and breakup ceases (due to the reduced relative velocity between the drops and the entrained gas).[31]

Measurements of droplet size distributions within a simulated diesel spray indicate how size varies with location. Figure 10-28 shows the variation in drop size distribution with radial distance from the spray axis, at a fixed axial location. The drop sizes were measured with a liquid immersion technique where a sample of drops is collected in a small cell filled with an immiscible liquid. Size distributions can be expressed in terms of:

1. The incremental number of drops $\Delta n$ within the size range $D_d - \Delta D_d/2 < D_d < D_d + \Delta D_d/2$
2. The incremental volume $\Delta V$ of drops in this size range
3. The cumulative number of drops $n$ less than a given size $D_d$
4. The cumulative volume $V$ of drops less than a given size $D_d$

Since the drops are spherical:

$$\frac{dn}{dD_d} = \frac{6}{\pi D_d^3} \frac{dV}{dD_d} \tag{10.29}$$

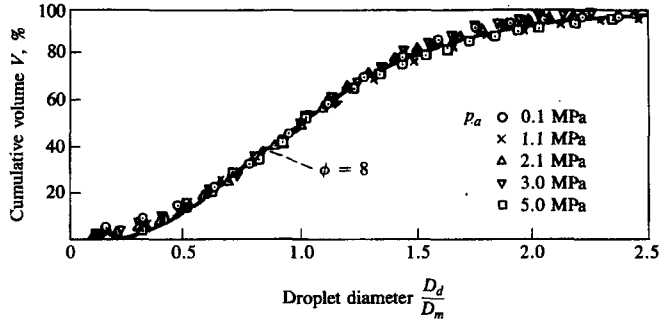


**FIGURE 10-29**
Normalized drop-size cumulative frequency distribution in spray injected into ambient-temperature air for air pressures from 0.1 to 5 MPa. Throttling pintle nozzle with nozzle opening pressure of 9.9 MPa. Median drop diameter $D_m = 1.224D_{SM}$.[32]

The distributions shown in the figure are frequency distributions of drop volume.[32] The peak in the distribution shifts to larger drop diameters as the radial position decreases: on average, the drops are smaller at the periphery of the spray.

To characterize the spray, expressions for drop size distribution and mean diameter are desirable. An appropriate and commonly used mean diameter is the *Sauter mean diameter:*

$$D_{SM} = \left(\int D_d^3\, dn\right) \Big/ \left(\int D_d^2\, dn\right) \tag{10.30}$$

where $dn$ is the number of drops with diameter $D_d$ in the range $D_d - dD_d/2 < D_d < D_d + dD_d/2$. The integration is usually carried out by summing over an appropriate number of drop size groups. The Sauter mean diameter is the diameter of the droplet that has the same surface/volume ratio as that of the total spray.

Various expressions for the distribution of drop sizes in liquid sprays have been proposed. One proposed by Hiroyasu and Kadota[32] based on the chi-square statistical distribution fits the available experimental data. Figure 10-29 shows how the chi-square distribution with a degree of freedom equal to 8 fits well to experimental measurements of the type shown in Fig. 10-28. Here $D_m$ is the median drop diameter which for this chi-square curve is $1.224D_{SM}$. The nondimensional expression for drop size distribution in sprays injected through hole nozzles, pintle nozzles, and throttling pintle nozzles given by the chi-square distribution is

$$\frac{dV}{V} = 13.5\left(\frac{D_d}{D_{SM}}\right)^3 \exp\left[-3\left(\frac{D_d}{D_{SM}}\right)\right] d\left(\frac{D_d}{D_{SM}}\right) \tag{10.31}$$



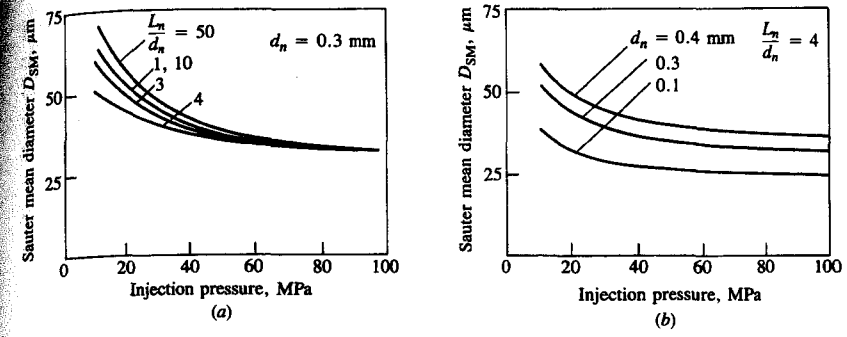


**FIGURE 10-30**
Effect of fuel-injection pressure and nozzle geometry and size on Sauter mean drop diameter. (*a*) Effect of nozzle length/diameter ratio $L_n/d_n$ and injection pressure. (*b*) Effect of nozzle diameter $d_n$ and injection pressure.[18]

An empirical expression for the Sauter mean diameter $D_{SM}$ (in micrometers) for typical diesel fuel properties given by Hiroyasu and Kadota[32] is

$$D_{SM} = A(\Delta p)^{-0.135}\rho_a^{0.121}V_f^{0.131} \tag{10.32}$$

where $\Delta p$ is the mean pressure drop across the nozzle in megapascals, $\rho_a$ is the air density in kilograms per cubic meter, and $V_f$ is the amount of fuel delivered per cycle per cylinder in cubic millimeters per stroke. $A$ is a constant which equals 25.1 for pintle nozzles, 23.9 for hole nozzles, and 22.4 for throttling pintle nozzles. Other expressions for predicting $D_{SM}$ can be found in Ref. 17.

The effects of injection pressure, nozzle geometry and size, air conditions, and fuel properties on Sauter mean diameter in sprays obtained with diesel fuel-injection nozzles have been extensively studied. Various immersion, photographic, and optical techniques for making such measurements have been used.[17] Some of the major effects are illustrated in Figs. 10-30 and 10-31 which show

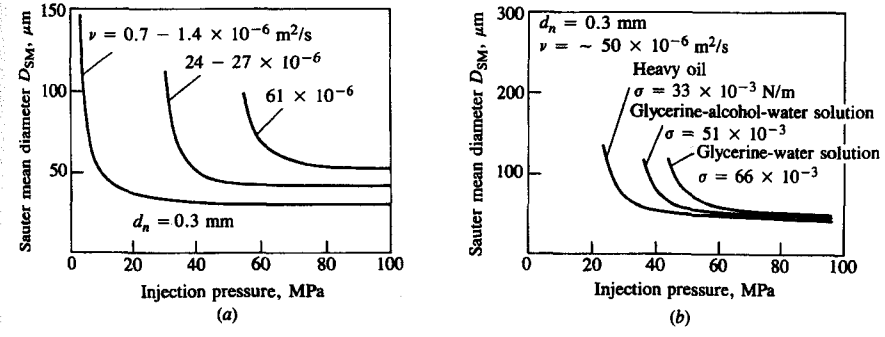


**FIGURE 10-31**
Effect of (*a*) liquid viscosity $\nu$ and (*b*) liquid surface tension $\sigma$ on Sauter mean drop diameter as a function of injection pressure. Air conditions: 3 MPa and ambient temperature.[17]

average Sauter mean diameters determined optically from studies of steady diesel fuel sprays in a pressurized vessel. Figure 10-30 shows that nozzle size affects the mean drop size in the expected direction. Nozzle length/diameter ratio is also shown to be important: an $L_n/d_n = 4$ gives the minimum mean drop size at low and intermediate injection pressures. This $L_n/d_n$ also corresponds to the minimum value of spray breakup length and to the maximum spray cone angle. Fuel viscosity and surface tension also affect mean drop size as shown in Fig. 10-31, with the effects being most significant at lower injection pressures.

### 10.5.6 Spray Evaporation

The injected liquid fuel, atomized into small drops near the nozzle exit to form a spray, must evaporate before it can mix with air and burn. Figure 10-20 showed the basic structure of an evaporating diesel spray under conditions typical of a large direct-injection engine. Back illumination showed that a core exists along the axis of the spray where the liquid fuel ligaments or drops are sufficiently dense to attenuate the light beam. Once the start-up phase of the injection process is over, the length of this core remains essentially constant until injection ends. This core is surrounded by a much larger vapor-containing spray region which continues to penetrate deeper into the combustion chamber: the core extends only partway to the spray tip. Additional insight into the physical structure of evaporating sprays can be obtained from the schlieren photographs taken just after the end of injection in a prechamber engine with air swirl, shown in Fig. 10-32. The lowest magnification picture (A) shows the overall structure of the spray. The only liquid-containing region evident is that part of the core nearest the nozzle which shows black on the left of the photograph. The spreading vapor region of the spray, carried around the chamber by the swirling air flow, appears mottled due to local turbulent vapor concentration and temperature fluctuations. The dark region within the spray vapor region is due to soot formed where the fuel vapor concentration is sufficiently high. It is probable that, after the breakup length, the dense black liquid core of the spray is composed of individual droplets but the concentration is so high along the optical path that the light beam is fully extinguished. However, the last part of the core close to the nozzle tip (B) disperses sufficiently for individual features to be resolved. The small black dots are liquid fuel drops in the size range 20 to 100 $\mu$m. Fuel drop vapor trails can be observed in the highest magnification photo (C) corresponding to various stages of evaporation. These range from drops showing little surrounding vapor to vapor trails with little liquid remaining at the head. The vapor trails show random orientations relative to the spray axis, presumably due to local air turbulence. The process of droplet evaporation under normal engine operating conditions appears to be rapid relative to the total combustion period.[21]

Let us examine the drop evaporation process in more detail. Consider a liquid drop at close to ambient temperature injected into air at typical end-of-compression engine conditions. Three phenomena will determine the history of the drop under these conditions:



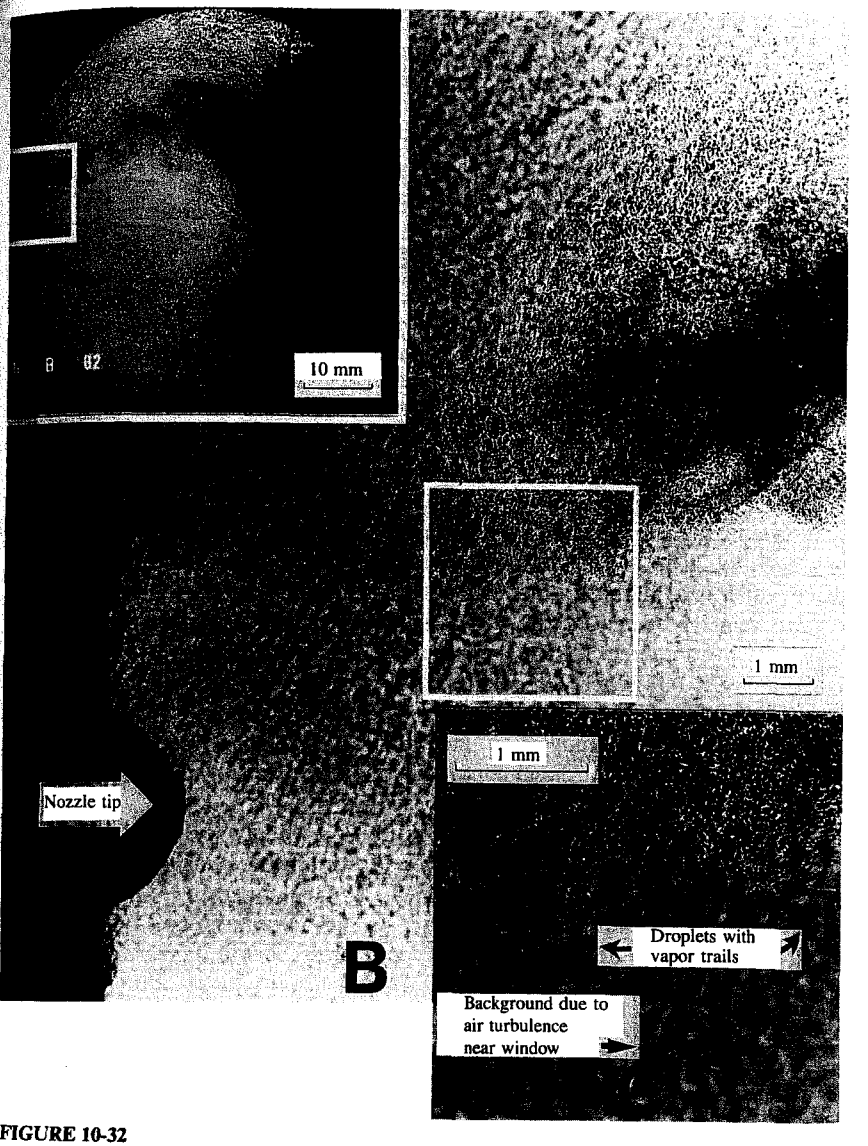


**FIGURE 10-32**
Shadowgraph photographs at three magnifications taken just after the end of injection of diesel-fuel spray into swirling air flow in prechamber of special diesel engine. Nozzle hole diameter = 0.25 mm.[21]

1. Deceleration of the drop due to aerodynamic drag
2. Heat transfer to the drop from the air
3. Mass transfer of vaporized fuel away from the drop

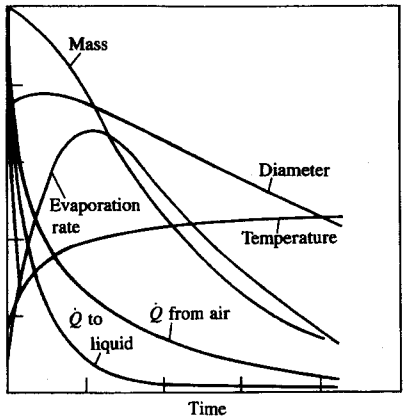


**FIGURE 10-33**
Schematic of variation of mass, diameter, temperature, evaporation rate, heat-transfer rate from air, and heat-transfer rate to liquid drop core as function of time during evaporation process of individual drop in diesel environment at the time of injection.

As the droplet temperature increases due to heat transfer, the fuel vapor pressure increases and the evaporation rate increases. As the mass transfer rate of vapor away from the drop increases, so the fraction of the heat transferred to the drop surface which is available to increase further the drop temperature decreases. As the drop velocity decreases, the convective heat-transfer coefficient between the air and the drop decreases. The combination of these factors gives the behavior shown in Fig. 10-33 where drop mass, temperature, velocity, vaporization rate, and heat-transfer rate from the air are shown schematically as a function of time following injection.[33] Analysis of individual fuel drops 25 $\mu$m in diameter, injected into air at typical diesel conditions, indicates that evaporation times are usually less than 1 ms.[34]

Such an analysis is relevant to drops that are widely separated (e.g., at the edge of the spray). In the spray core, where drop number densities are high, the evaporation process has a significant effect on the temperature and fuel-vapor concentration in the air within the spray. As fuel vaporizes, the local air temperature will decrease and the local fuel vapor pressure will increase. Eventually thermodynamic equilibrium would pertain: this is usually called adiabatic saturation.[33] Calculated thermodynamic equilibrium temperatures for diesel spray conditions are plotted in Fig. 10-34 as a function of the fuel/air mass ratio for *n*-dodecane and *n*-heptane. The initial liquid fuel temperature was 300 K. The ratio of fuel vapor to air mass at these equilibrium conditions is also shown. To the left of the peaks in the $m_{fv}/m_a$ curves, only fuel vapor is present. To the right of these peaks, liquid fuel is also present because the vapor phase is saturated.[35] Liquid fuel vaporization causes substantial reductions in gas temperature. While this equilibrium situation may not be reached within the spray, these results are useful for understanding the temperature distribution within an evaporating spray.

To quantify accurately the fuel vaporization rate within a diesel fuel spray requires the solution of the coupled conservation equations for the liquid drop-



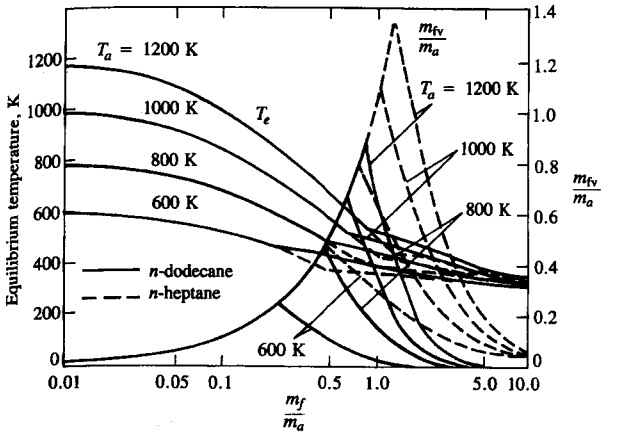


**FIGURE 10-34**
Adiabatic-saturation conditions for equilibrium mixtures formed by injecting *n*-dodecane and *n*-heptane, initially liquid at 300 K, into air at initial temperature $T_a$ between 600 and 1200 K and initial density 6.5 kg/m$^3$. Equilibrium mixture temperature ($T_e$) and ratio of fuel vapor mass ($m_{fv}$) to air mass ($m_a$) shown as function of ratio of total fuel mass $m_f$ to $m_a$. Fuel vapor only present to left of peaks in $m_{fv}/m_a$ curves: liquid fuel also present to right of peaks.[35]

lets and the air within the combustion chamber. Various phenomenological models and computational fluid dynamic models have been developed for this purpose (see Secs. 14.4.3 and 14.5.5). In the most sophisticated of these, the spray is assumed to be composed of discrete computational particles each of which represents a group of droplets of similar size, temperature, etc. The distribution functions in droplet size, velocity, temperature, etc., produced by the fuel injector are statistically sampled and the resulting discrete particles are followed along lagrangian trajectories as they interact and exchange mass, momentum, and energy with the surrounding gas. Drops interact directly with each other via collisions and indirectly via evaporation by modifying the ambient vapor concentration and gas temperature. Studies with such models indicate that, under normal diesel engine conditions, 70 to 95 percent of the injected fuel is in the vapor phase at the start of combustion. Evaporation is more than 90 percent complete after 1 ms. However, only 10 to 35 percent of the vaporized fuel has mixed to within flammability limits in a typical medium-speed DI diesel engine. Thus combustion is largely mixing-limited, rather than evaporation-limited.[36] Of course, under cold-starting conditions, evaporation becomes a major constraint.

## 10.6 IGNITION DELAY

### 10.6.1 Definition and Discussion

The ignition delay in a diesel engine was defined as the time (or crank angle) interval between the start of injection and the start of combustion. The start of

injection is usually taken as the time when the injector needle lifts off its seat (determined by a needle-lift indicator). The start of combustion is more difficult to determine precisely. It is best identified from the change in slope of the heat-release rate, determined from cylinder pressure data using the techniques described in Sec. 10.4, which occurs at ignition. Depending on the character of the combustion process, the pressure data alone may indicate when pressure change due to combustion first occurs; in DI engines under normal conditions ignition is well defined, but in IDI engines the ignition point is harder to identify. Flame luminosity detectors are also used to determine the first appearance of the flame. Experience has shown that under normal conditions, the point of appearance of the flame is later than the point of pressure rise and results in greater uncertainty or error in determining the ignition point.

Both physical and chemical processes must take place before a significant fraction of the chemical energy of the injected liquid fuel is released. The physical processes are: the atomization of the liquid fuel jet; the vaporization of the fuel droplets; the mixing of fuel vapor with air. The chemical processes are the precombustion reactions of the fuel, air, residual gas mixture which lead to autoignition. These processes are affected by engine design and operating variables, and fuel characteristics, as follows.

Good atomization requires high fuel-injection pressure, small injector hole diameter, optimum fuel viscosity, and high cylinder air pressure at the time of injection (see Sec. 10.5.3). The rate of vaporization of the fuel droplets depends on the size of the droplets, their distribution, and their velocity, the pressure and temperature inside the chamber, and the volatility of the fuel. The rate of fuel-air mixing is controlled largely by injector and combustion chamber design. Some combustion chamber and piston head shapes are designed to amplify swirl and create turbulence in the air charge during compression. Some engine designs use a prechamber or swirl chamber to create the vigorous air motion necessary for rapid fuel-air mixing (see Sec. 10.2). Also, injector design features such as the number and spatial arrangement of the injector holes determine the fuel spray pattern. The details of each nozzle hole affect the spray cone angle. The penetration of the spray depends on the size of the fuel droplets, the injection pressure, the air density, and the air-flow characteristics. The arrangement of the sprays, the spray cone angle, the extent of spray penetration, and the air flow all affect the rate of air entrainment into the spray. These physical aspects of fuel-injection and fuel-spray behavior are reviewed in Sec. 10.5.

The chemical component of the ignition delay is controlled by the precombustion reactions of the fuel. A fundamental discussion of autoignition or spontaneous hydrocarbon oxidation in premixed fuel-air mixtures is given in Sec. 9.6.2. Since the diesel engine combustion process is heterogeneous, its spontaneous ignition process is even more complex. Though ignition occurs in vapor phase regions, oxidation reactions can proceed in the liquid phase as well between the fuel molecules and the oxygen dissolved in the fuel droplets. Also, cracking of large hydrocarbon molecules to smaller molecules is occurring. These chemical processes depend on the composition of the fuel and the cylinder charge temperature and pressure, as well as the physical processes described above which govern the distribution of fuel throughout the air charge.



Since the ignition characteristics of the fuel affect the ignition delay, this property of a fuel is very important in determining diesel engine operating characteristics such as fuel conversion efficiency, smoothness of operation, misfire, smoke emissions, noise, and ease of starting. The ignition quality of a fuel is defined by its cetane number. Cetane number is determined by comparing the ignition delay of the fuel with that of primary reference fuel mixtures in a standardized engine test (see below). For low cetane fuels with too long an ignition delay, most of the fuel is injected before ignition occurs, which results in very rapid burning rates once combustion starts with high rates of pressure rise and high peak pressures. Under extreme conditions, when autoignition of most of the injected fuel occurs, this produces an audible knocking sound, often referred to as "diesel knock." For fuels with very low cetane numbers, with an exceptionally long delay, ignition may occur sufficiently late in the expansion process for the burning process to be quenched, resulting in incomplete combustion, reduced power output, and poor fuel conversion efficiency. For higher cetane number fuels, with shorter ignition delays, ignition occurs before most of the fuel is injected. The rates of heat release and pressure rise are then controlled primarily by the rate of injection and fuel-air mixing, and smoother engine operation results.

### 10.6.2 Fuel Ignition Quality

The ignition quality of a diesel fuel is defined by its *cetane number*. The method used to determine the ignition quality in terms of cetane number is analogous to that used for determining the antiknock quality of gasoline in terms of octane number. The cetane number scale is defined by blends of two pure hydrocarbon reference fuels. Cetane (*n*-hexadecane, $C_{16}H_{34}$), a hydrocarbon with high ignition quality, represents the top of the scale with a cetane number of 100. An isocetane, heptamethylnonane (HMN), which has a very low ignition quality, represents the bottom of the scale with a cetane number of 15.† Thus, cetane number (CN) is given by

$$\text{CN} = \text{percent } n\text{-cetane} + 0.15 \times \text{percent HMN} \tag{10.33}$$

The engine used in cetane number determination is a standardized single-cylinder, variable compression ratio engine with special loading and accessory equipment and instrumentation. The engine, the operating conditions, and the test procedure are specified by ASTM Method D613.[37] The operating requirements include: engine speed—900 rev/min; coolant temperature—100°C; intake air temperature—65.6°C (150°F); injection timing—13° BTC; injection

† In the original procedure α-methylnapthalene ($C_{11}H_{10}$) with a cetane number of zero represented the bottom of the scale. Heptamethylnonane, a more stable compound, has replaced it.

pressure—10.3 MPa (1500 lb/in$^2$). With the engine operating under these conditions, on the fuel whose cetane number is to be determined, the compression ratio is varied until combustion starts at TC: i.e., an ignition delay period of 13° (2.4 ms at 900 rev/min) is produced. The above procedure is then repeated using reference fuel blends. Each time a reference fuel is tried, the compression ratio is adjusted to give the same 13° ignition delay. When the compression ratio required by the actual fuel is bracketed by the values required by two reference blends differing by less than five cetane numbers, the cetane number of the fuel is determined by interpolation between the compression ratios required by the two reference blends.

Because of the expense of the cetane number test, many correlations which predict ignition quality based on the physical properties of diesel fuels have been developed.[38, 39] A calculated *cetane index* (CCI) is often used to estimate ignition quality of diesel fuels (ASTM D976[40]). It is based on API gravity and the mid-boiling point (temperature 50 percent evaporated). It is applicable to straight-run fuels, catalytically cracked stocks, and blends of the two. Its use is suitable for most diesel fuels and gives numbers that correspond quite closely to cetane number. A *diesel index* is also used. It is based on the fact that ignition quality is linked to hydrocarbon composition: *n*-paraffins have high ignition quality, and aromatic and napthenic compounds have low ignition quality. The aniline point (ASTM D611[41]—the lowest temperature at which equal volumes of the fuel and aniline become just miscible) is used, together with the API gravity, to give the diesel index:

$$\text{Diesel index} = \text{aniline point (°F)} \times \frac{\text{API gravity}\dagger}{100} \tag{10.34}$$

The diesel index depends on the fact that aromatic hydrocarbons mix completely with aniline at comparatively low temperatures, whereas paraffins require considerably higher temperatures before they are completely miscible. Similarly, a high API gravity denotes low specific gravity and high paraffinicity, and, again, good ignition quality. The diesel index usually gives values slightly above the cetane number. It provides a reasonable indication of ignition quality in many (but not all) cases.

### 10.6.3 Autoignition Fundamentals

Basic studies in constant-volume bombs, in steady-flow reactors, and in rapid-compression machines have been used to study the autoignition characteristics of fuel-air mixtures under controlled conditions. In some of these studies the fuel and air were premixed; in some, fuel injection was used. Studies with fuel injection into constant-temperature and pressure environments have shown that the temperature and pressure of the air are the most important variables for a given fuel composition. Ignition delay data from these experiments have usually been correlated by equations of the form:

$$\tau_{id} = Ap^{-n} \exp\left(\frac{E_A}{\bar{R}T}\right) \tag{10.35}$$

where $\tau_{id}$ is the ignition delay (the time between the start of injection and the start of detectable heat release), $E_A$ is an apparent activation energy for the fuel autoignition process, $\bar{R}$ is the universal gas constant, and $A$ and $n$ are constants dependent on the fuel (and, to some extent, the injection and air-flow characteristics).

Figure 10-35*a* shows ignition delay data obtained by injecting liquid fuel sprays into a high-pressure heated constant-volume bomb.[42] Figure 10-35*b* shows ignition delay data from a steady-flow high-pressure reactor where vaporized fuel was mixed rapidly with the heated air stream.[43] The match between the form of Eq. (10.35) and the data is clear. Figure 10-35*b* also shows an equivalence ratio dependence of the ignition delay. Representative values for $A$, $n$, and $E_A$ for Eq. (10.35), taken from these and other studies, are given in Table 10.3. Ignition delay times calculated with these formulas for various diesel engines are given in

† API gravity is based on specific gravity and is calculated from: API gravity, deg = (141.5/specific gravity at 60°F) − 131.5.



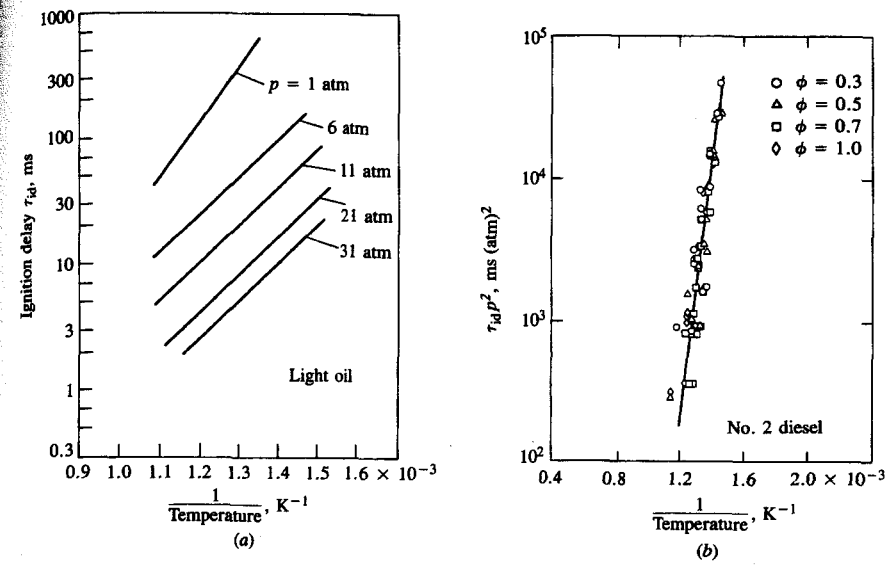


**FIGURE 10-35**
(*a*) Ignition delay as function of reciprocal air temperature for light oil spray injected into constant-volume combustion bomb. Injection pressure 9.8 MPa (100 atm). Air pressures indicated.[42] (*b*) Ignition delay × (pressure)$^2$ measured in steady-flow reactor for No. 2 diesel fuel as function of reciprocal temperature. Fuel/air equivalence ratio $\phi$ varied from 0.3 to 1.0.[43]

TABLE 10.3
**Constants for Arrhenius equation for ignition delay:[44]**

$$\tau_{id}(\text{ms}) = Ap^{-n} \exp\,[E_A/(\bar{R}T)]$$

| | Conditions | | | | Parameters | | |
|---|---|---|---|---|---|---|---|
| Investigator | Apparatus | Fuel | $p$, atm | $T$, K | $n$ | $A$ | $E_A/\bar{R}$, K |
| Spadaccini and TeVelde[43] No. 1 | Steady flow | No. 2 diesel | 10–30 | 650–900 | 2 | $2.43 \times 10^{-9}$ | 20,926 |
| Spadaccini and TeVelde[43] No. 2 | Steady flow | No. 2 diesel | 10–30 | 650–900 | 1 | $4.00 \times 10^{-10}$ | 20,080 |
| Stringer *et al.*[45] | Steady flow | Diesel 45–50 cetane number | 30–60 | 770–980 | 0.757 | 0.0405 | 5,473 |
| Wolfer[46] | Constant-volume bomb | Fuel with cetane number >50 | 8–48 | 590–782 | 1.19 | 0.44 | 4,650 |
| Hiroyasu *et al.*[29] | Constant-volume bomb | Kerosene | 1–30 | 673–973 | 1.23 | 0.0276 | 7,280 |

Table 10.4. Air pressures and temperatures at TC piston position were estimated from measured cylinder pressure data. Measured ignition delay times in these types of engines are: 0.6 to 3 ms for low-compression-ratio DI diesel engines over a wide range of operating conditions; 0.4 to 1 ms for high-compression-ratio and turbocharged DI diesel engines; 0.6 to 1.5 ms for IDI diesel engines.[44]

The variation in the calculated delay times can be attributed to several factors:

1. In some cases the correlations are being extrapolated outside their original range of operating conditions.
2. The methods used to detect the start of combustion, and hence the duration of the delay, are not identical.
3. The experimental apparatus and the method of fuel-air mixture preparation are different.

The third factor is probably the most significant. As has been explained, the phenomenon of autoignition of a fuel spray consists of sequences of physical and chemical processes of substantial complexity. The relative importance of each process depends on the ambient conditions, on fuel properties, and on how the fuel-air mixture is prepared. For example, fuel evaporation times are significant in cold engines, but not under fully warmed-up conditions. Thus, an equation of the simple form of Eq. (10.35) can only fit the data over a limited range of conditions. The correlations of Spadaccini and TeVelde[43] have much higher activation energies. Normally, lower values of $E_A/\bar{R}$ imply that physical processes such as vaporization and mixing are important and relevant to chemical processes. Thus, fuel preparation, mixture inhomogeneity, heat loss, and nonuniform flow patterns



TABLE 10.4
**Calculated ignition delay times[44]**

| | Conditions | | | $\tau_{id}$, ms | | | | |
|---|---|---|---|---|---|---|---|---|
| | | | | Spadaccini and TeVelde[43] | | | | |
| Engine | Speed, rev/min | $p$, atm | $T$, K | No. 1 | No. 2 | Stringer *et al.*[45] | Wolfer[46] | Hiroyasu *et al.*[29] |
| IDI Diesel | | | | | | | | |
| 1. Low swirl | 600 | 45.6 | 690 | 17.3 | 38.2 | 6.26 | 3.94 | 9.60 |
| | 1200 | 49.3 | 747 | 1.47 | 3.83 | 3.22 | 2.15 | 3.90 |
| | 1800 | 52.5 | 758 | 0.86 | 2.44 | 2.76 | 1.82 | 3.13 |
| 2. High swirl | 600 | 45.2 | 674 | 36.3 | 76.9 | 7.60 | 4.68 | 12.5 |
| | 1200 | 48.4 | 721 | 4.18 | 10.3 | 4.25 | 2.75 | 5.67 |
| | 1800 | 51.8 | 744 | 1.47 | 4.07 | 3.19 | 2.08 | 3.82 |
| DI Diesel | | | | | | | | |
| 1. Low compression ratio | | 42.8 | 781 | 0.57 | 1.37 | 2.60 | 1.92 | 2.39 |
| 2. High compression ratio | 1500 | 58.8 | 975 | 0.0015 | 0.0060 | 0.508 | 0.407 | 0.322 |

affect the ignition delay. While the work of Spadaccini and TeVelde probably describes the chemical ignition delay more accurately, since great care was taken to obtain a uniform mixture and flow, the experiments in constant-volume bombs with diesel-type fuel injectors are more relevant to the diesel engine compression-ignition combustion process because they include the appropriate physical and chemical processes. The available engine ignition delay data suggest that for delays less than about 1 ms, the rate of decrease in delay with increasing temperature becomes much less than that indicated by the data in Fig. 10-35. This is due to the increasing relative importance of physical processes relative to chemical processes during the delay period. Thus relations of the form of Eq. (10.35) should be used with caution.

In general, $\tau_{id}$ is a function of mixture temperature, pressure, equivalence ratio, and fuel properties (though no accepted form for the variation with equivalence ratio is yet established). In the above referenced studies, the fuel was injected into a uniform air environment where the pressure and temperature only changed due to the cooling effect of the fuel-vaporization and fuel-heating processes. In an engine, pressure and temperature change during the delay period due to the compression resulting from piston motion. To account for the effect of changing conditions on the delay the following empirical integral relation is usually used:

$$\int_{t_{si}}^{t_{si}+\tau_{id}} \left(\frac{1}{\tau}\right) dt = 1 \tag{10.36}$$

where $t_{si}$ is the time of start of injection, $\tau_{id}$ is the ignition delay period, and $\tau$ is the ignition delay at the conditions pertaining at time $t$. Whether the variation in conditions is significant depends on the amount of injection advance before TC that is used and the length of the delay.

**TABLE 10.5**
**Effects of engine design and operating variables on heat-release rates**

| Reference | Parameter varied | Effect on $\tau_{id}$ | $\dot{m}_m$ | $\dot{Q}_p$ | $\dot{Q}_m$ |
|---|---|---|---|---|---|
| 5, 64 | Injection rate ↑ | * | ↑ | ↑ | ↑ |
| 65 | Turbocharger boost ↑ | ↓ | * | ↓ | * |
| 66 | Compression ratio ↓ | ↑ | * | ↑ | * |
| 66 | Number of injector holes ↑ | * | ↑ | ↑ | ↑ |
| 67, 68 | Injection advance ↑ | ↑ | * | ↑ | * |
| 67, 68 | Swirl ↑ | * | ↑ | ↑ | ↑ |
| 67 | Intake-air temperature ↓ | ↑ | * | ↑ | * |
| 68, 69 | Injection pressure ↑ | * | ↑ | ↑ | ↑ |
| 11, 69 | Speed ↑ | * | ↑ | ↑ | ↑ |

$\tau_{id}$, ignition delay; $\dot{m}_m = (dm/dt)_m$, fuel-air mixing rate; $\dot{Q}_p = (dQ/dt)_p$, heat-release rate during premixed-combustion phase; $\dot{Q}_m = (dQ/dt)_m$, heat-release rate during mixing-controlled-combustion phase. ↑ increase; ↓ decrease; * minor effect.
*Source:* From Plee and Ahmad.[44]

## PROBLEMS

**10.1.** Describe the sequence of processes which must occur before the liquid fuel in the injection system in a direct-injection compression-ignition engine is fully burned.

**10.2.** Small high-swirl direct-injection CI engines have fuel conversion efficiencies which are about 10 percent higher than values typical of equivalent indirect-injection engines. (IDI engines are used because they achieve higher bmep.) What combustion-system-related differences contribute to this higher efficiency?

**10.3.** In a diesel engine, because the fuel distribution is nonuniform the burned gas temperature is nonuniform. Consider small fuel-air mixture elements initially at 1000 K and 6.5 MPa at top-center with a range of equivalence ratios. Each element burns at essentially constant pressure. Calculate (using the charts in Chap. 4, or an appropriate chemical equilibrium thermodynamic computer code) the burned gas temperature for mixture equivalence ratios of 0.4, 0.6, 0.8, 1.0, 1.2. Assume the fuel is isooctane.

**10.4.** The levels of combustible species in the exhaust of a direct-injection diesel engine are: HC, 0.8 g/kW · h; CO, 3 g/kW · h; particulates, 0.7 g/kW · h. If the specific fuel consumption is 210 g/kW · h calculate the combustion efficiency.

**10.5.** Consider the naturally aspirated direct-injection diesel engine in Fig. 1-23 operating at 2300 rev/min and an equivalence ratio of 0.7. Estimate the following:
(*a*) Mass of air in each cylinder per cycle, mass, and volume (as liquid) of diesel fuel injected per cylinder per cycle.
(*b*) Estimate the average drop size [e.g., use Eq. (10.32)]. The cylinder pressure at time of injection (close to TC) is 50 atm; the fuel injection pressure is 500 atm.
(*c*) Assuming all fuel droplets are the same size as the average drop, how many drops are produced per injection? If these drops are uniformly distributed throughout the air charge at TC, what is the approximate distance between drops? (Neither of these assumptions is correct; however, the calculations illustrate the difficulty of the fuel-air mixing process.)



**10.6.** Estimate the following quantities for a typical direct-injection diesel fuel spray. The injection pressure is 500 atm; the cylinder pressure during injection is 50 atm.
(*a*) Assuming that the flow through the nozzle orifice is incompressible and quasi steady, estimate the liquid fuel velocity at the orifice exit. At this velocity, how long would the fuel take to reach the cylinder wall? The bore is 125 mm.
(*b*) Each nozzle orifice diameter $d_n$ is 0.34 mm and $L_n/d_n = 4$. Determine the spray angle and plot spray tip penetration versus time.
(*c*) Use Eq. (10.32) to estimate the initial average drop size assuming that the injection process in (*a*) above continues for 1 millisecond and the injector nozzle has four orifices.

**10.7.** Diesel fuel is injected as a liquid at room temperature into air at 50 atm and 800 K, close to TC at the end of compression. If the overall equivalence ratio is 0.7, estimate the reduction in average air temperature which would occur when the fuel is fully vaporized and uniformly mixed. Assume such mixing takes place at constant volume prior to any combustion.

**10.8.** Using Eq. (10.37) estimate the ignition delay in milliseconds and crank angle degrees for these operating conditions in Table 10.4: low swirl IDI diesel 600 and 1800 rev/min; high swirl IDI diesel 1800 rev/min; DI diesel low and high compression ratio. The fuel cetane number is 45; stroke = 0.1 m. Discuss whether the predicted trends with speed, swirl, and compression ratio are consistent with Sec. 10.6.4.

**10.9.** The compression ratio of truck diesel engines must be set at about 18 so that the engine will start when cold. Using Eqs. (10.37) to (10.39) develop a graph of $\tau_{id}$ (in degrees) as a function of compression ratio for $r_c = 12$ to 20. Assume $p_i = 1$ atm, $T_i = 255$ K, $n = 1.13$, speed = 100 rev/min, bore = stroke = 120 mm, fuel cetane number = 45. If the ignition delay must be less than 20° CA for satisfactory starting, what compression ratio is required?

**10.10.** Equation (10.40) predicts the fraction $\beta$ of the fuel injected into a direct-injection diesel engine which burns in the premixed phase. Plot $\beta$ as a function of $\tau_{id}$ for $\phi = 0.4$. Show that for turbocharged DI diesel engines where $\tau_{id}$ is 0.4 to 1 ms, the premixed combustion phase is much less important than it normally is for naturally aspirated engines where $\tau_{id}$ is between 0.7 and 3 ms.

## REFERENCES


1. Alcock, J. F., and Scott, W. M.: "Some More Light on Diesel Combustion," *Proc. Auto. Div., Instn Mech. Engrs*, No. 5, pp. 179–191, 1962–1963.
2. Scott, W. M.: "Understanding Diesel Combustion through the Use of High Speed Moving Pictures in Color," SAE paper 690002, *SAE Trans.*, vol. 78, 1969.
3. Neitz, A., and D'Alfonso, N.: "The M.A.N. Combustion System with Controlled Direct Injection for Passenger Car Diesel Engines," SAE paper 810479, 1979.
4. Ogasawara, M., Tokunaga, Y., Horio, K., Uryu, M., and Hirofumi, N.: "Photographic Study on the Intermittent Spray Combustion by a Rapid Compression Machine" (in Japanese), *Internal Combustion Engine*, vol. 15, 1976.
5. Austen, A. E. W., and Lyn, W.-T.: "Relation between Fuel Injection and Heat Release in a Direct-Injection Engine and the Nature of the Combustion Processes," *Proc. Instn Mech. Engrs*, No. 1, pp. 47–62, 1960–1961.
6. Lyn, W.-T.: "Study of Burning Rate and Nature of Combustion in Diesel Engines," in *Proceedings of Ninth International Symposium on Combustion*, pp. 1069–1082, The Combustion Institute, 1962.
7. Cheng, W., and Gentry, R.: "Effects on Charge Non-Uniformity on Diesel Heat Release Analysis," SAE paper 861568, 1986.

8. Gatowski, J. A., Balles, E. N., Chun, K. M., Nelson, F. E., Ekchian, J. A., and Heywood, J. B.: "Heat Release Analysis of Engine Pressure Data," SAE paper 841359, *SAE Trans.*, vol. 93, 1984.
9. Krieger, R. B., and Borman, G. L.: "The Computation of Apparent Heat Release for Internal Combustion Engines," ASME paper 66-WA/DGP-4, in *Proc. Diesel Gas Power*, ASME, 1966.
10. Watson, N., and Kamel, M.: "Thermodynamic Efficiency Evaluation of an Indirect Injection Diesel Engine," SAE paper 790039, *SAE Trans.*, vol. 88, 1979.
11. Kort, R. T., Mansouri, S. H., Heywood, J. B., and Ekchian, J. A.: "Divided-Chamber Diesel Engine, Part II: Experimental Validation of a Predictive Cycle-Simulation and Heat Release Analysis," SAE paper 820274, *SAE Trans.*, vol. 91, 1982.
12. Obert, E. F.: *Internal Combustion Engines and Air Pollution*, Intext Educational Publishers, 1973 edition.
13. Weathers, Jr., T., and Hunter, C.: *Diesel Engines for Automobiles and Small Trucks*, Reston Publishing Company, a Prentice-Hall Company, Reston, Va. 1981.
14. Bosch: *Automotive Handbook*, 1st English ed., Robert Bosch GmbH, 1976.
15. Williams, Jr., H. A.: "The GM/EMD Model 710G Series Engine," in *Marine Engine Development*, SP-625, SAE, 1985. Also ASME paper 85-GGP-24, 1985.
16. Hames, R. J., Straub, R. D., and Amann, R. W.: "DDEC Detroit Diesel Electronic Control," SAE paper 850542, 1985.
17. Hiroyasu, H.: "Diesel Engine Combustion and Its Modeling," in *Diagnostics and Modeling of Combustion in Reciprocating Engines*, pp. 53–75, COMODIA 85, Proceedings of Symposium, Tokyo, Sept. 4–6, 1985.
18. Arai, M., Tabata, M., and Hiroyasu, H.: "Disintegrating Process and Spray Characterization of Fuel Jet Injected by a Diesel Nozzle," SAE paper 840275, *SAE Trans.*, vol. 93, 1984.
19. Kamimoto, T., Kobayashi, H., and Matsuoka, S.: "A Big Size Rapid Compression Machine for Fundamental Studies of Diesel Combustion," SAE paper 811004, *SAE Trans.*, vol. 90, 1981.
20. Balles, E.: "Fuel-Air Mixing and Diesel Combustion in a Rapid Compression Machine," Ph.D. Thesis, Department of Mechanical Engineering, MIT, June 1987.
21. Browne, K. R., Partridge, I. M., and Greeves, G.: "Fuel Property Effects on Fuel/Air Mixing in an Experimental Diesel Engine," SAE paper 860223, 1986.
22. Bracco, F. V.: "Modeling of Engine Sprays," SAE paper 850394, 1985.
23. Kuo, T., and Bracco, F. V.: "Computations of Drop Sizes in Pulsating Sprays and of Liquid-Core Length in Vaporizing Sprays," SAE paper 820133, *SAE Trans.*, vol. 91, 1982.
24. Reitz, R. D., and Bracco, F. V.: "Mechanism of Atomization of a Liquid Jet," *Phys. Fluid*, vol. 25, no. 10, pp. 1730–1742, 1982.
25. Reitz, R. D., and Bracco, F. V.: "On the Dependence of Spray Angle and Other Spray Parameters on Nozzle Design and Operating Conditions," SAE paper 790494, 1979.
26. Wu, K.-J., Su, C.-C., Steinberger, R. L., Santavicca, D. A., and Bracco, F. V.: "Measurements of the Spray Angle of Atomizing Jets," *J. Fluids Engng*, vol. 105, pp. 406–413, 1983.
27. Hay, N., and Jones, P. L.: "Comparison of the Various Correlations for Spray Penetration," SAE paper 720776, 1972.
28. Dent, J. C.: "Basis for the Comparison of Various Experimental Methods for Studying Spray Penetration," SAE paper 710571, *SAE Trans.*, vol. 80, 1971.
29. Hiroyasu, H., Kadota, T., and Arai, M.: "Supplementary Comments: Fuel Spray Characterization in Diesel Engines," in James N. Mattavi and Charles A. Amann (eds.), *Combustion Modeling in Reciprocating Engines*, pp. 369–408, Plenum Press, 1980.
30. Wu, K.-J., Reitz, R. D., and Bracco, F. V.: "Measurements of Drop Size at the Spray Edge near the Nozzle in Atomizing Liquid Jets," *Phys. Fluids*, vol. 29, no. 4, pp. 941–951, 1986.
31. Reitz, R. D., and Diwakar, R.: "Effect of Drop Breakup on Fuel Sprays," SAE paper 860469, 1986.
32. Hiroyasu, H., and Kadota, T.: "Fuel Droplet Size Distribution in Diesel Combustion Chamber," SAE paper 740715, *SAE Trans.*, vol. 83, 1974.
33. El Wakil, M. M., Myers, P. S., and Uyehara, O. A.: "Fuel Vaporization and Ignition Lag in Diesel Combustion," in *Burning a Wide Range of Fuels in Diesel Engines, SAE Progress in Technol.*, vol. 11, pp. 30–44, SAE, 1967.





34. Borman, G. L., and Johnson, J. H.: "Unsteady Vaporization Histories and Trajectories of Fuel Drops Injected into Swirling Air," in *Burning a Wide Range of Fuels in Diesel Engines, SAE Progress in Technology*, vol. 11, pp. 13–29, SAE, 1967; also SAE paper 598C, 1962.
35. Kamimoto, T., and Matsuoka, S.: "Prediction of Spray Evaporation in Reciprocating Engines," SAE paper 770413, *SAE Trans.*, vol. 86, 1977.
36. Kuo, T., Yu, R. C., and Shahed, S. M.: "A Numerical Study of the Transient Evaporating Spray Mixing Process in the Diesel Environment," SAE paper 831735, *SAE Trans.*, vol. 92, 1983.
37. ASTM Method D613, Cetane Test Procedure.
38. Henein, N. A., and Fragoulis, A. N.: "Correlation between Physical Properties and Autoignition Parameters of Alternate Fuels," SAE paper 850266, 1985.
39. Gulder, O. L., Glavincevski, B., and Burton, G. F.: "Ignition Quality Rating Methods for Diesel Fuels—A Critical Appraisal," SAE paper 852080, 1985.
40. ASTM D976, Calculated Cetane Index.
41. ASTM D611.
42. Igura, S., Kadota, T., and Hiroyasu, H.: "Spontaneous Ignition Delay of Fuel Sprays in High Pressure Gaseous Environments," *Trans. Japan Soc. Mech. Engrs*, vol. 41, no. 345, pp. 24–31, 1975.
43. Spadaccini, L. J., and TeVelde, J. A.: "Autoignition Characteristics of Aircraft-Type Fuels," *Combust. Flame*, vol. 46, pp. 283–300, 1982.
44. Plee, S. L., and Ahmad, T.: "Relative Roles of Premixed and Diffusion Burning in Diesel Combustion," SAE paper 831733, *SAE Trans.*, vol. 92, 1983.
45. Stringer, F. W., Clarke, A. E., and Clarke, J. S.: "The Spontaneous Ignition of Hydrocarbon Fuels in a Flowing System," *Proc. Instn Mech. Engrs*, vol. 184, pt. 3J, 1969–1970.
46. Wolfer, H. H.: "Ignition Lag in Diesel Engines," VDI-Forschungsheft 392, 1938; Translated by Royal Aircraft Establishment, Farnborough Library No. 358, UDC 621–436.047, August 1959.
47. Lyn, W.-T., and Valdmanis, E.: "Effects of Physical Factors on Ignition Delay," SAE paper 680102, 1968.
48. Wong, C. L., and Steere, D. E.: "The Effects of Diesel Fuel Properties and Engine Operating Conditions on Ignition Delay," SAE paper 821231, *SAE Trans.*, vol. 91, 1982.
49. Andree, A., and Pachernegg, S. J.: "Ignition Conditions in Diesel Engines," SAE paper 690253, *SAE Trans.*, vol. 78, 1969.
50. Glavincevski, B., Gülder, O. L., and Gardner, L.: "Cetane Number Estimation of Diesel Fuels from Carbon Type Structural Composition," SAE paper 841341, 1984.
51. Olree, R., and Lenane, D.: "Diesel Combustion Cetane Number Effects," SAE paper 840108, *SAE Trans.*, vol. 93, 1984.
52. Schaefer, A. J., and Hardenberg, H. O.: "Ignition Improvers for Ethanol Fuels," SAE paper 810249, *SAE Trans.*, vol. 90, 1981.
53. Hardenberg, H. O., and Hase, F. W.: "An Empirical Formula for Computing the Pressure Rise Delay of a Fuel from its Cetane Number and from the Relevant Parameters of Direct-Injection Diesel Engines," SAE paper 790493, *SAE Trans.*, vol. 88, 1979.
54. Dent, J. C., and Mehta, P. S.: "Phenomenological Combustion Model for a Quiescent Chamber Diesel Engine," SAE paper 811235, *SAE Trans.*, vol. 90, 1981.
55. Chang, Y. J., Kobayashi, H., Matsuzawa, K., and Kamimoto, T.: "A Photographic Study of Soot Formation and Combustion in a Diesel Flame with a Rapid Compression Machine," in *Diagnostics and Modeling of Combustion in Reciprocating Engines*, pp. 149–157, COMODIA 85, Proceedings of Symposium, Tokyo, Sept. 4–6, 1985.
56. Lakshminarayan, P. A., and Dent, J. C.: "Interferometric Studies of Vaporising and Combustion Sprays," SAE paper 830244, *SAE Trans.*, vol. 92, 1983.
57. Colella, K. J., Balles, E. N., Ekchian, J. A., Cheng, W. K., and Heywood, J. B.: "A Rapid Compression Machine Study of the Influence of Charge Temperature on Diesel Combustion," SAE paper 870587, 1987.
58. Morris, C. J., and Dent, J. C.: "The Simulation of Air Fuel Mixing in High Swirl Open Chamber Diesel Engines," *Proc. Instn Mech. Engrs*, vol. 190, no. 47/76, pp. 503–513, 1976.
59. Rife, J., and Heywood, J. B.: "Photographic and Performance Studies of Diesel Combustion with